3-27-2024

INVESTIGATION OF GAS DYNAMICS IN WATER AND OIL-BASED MUDS USING DAS, DTS, AND DSS MEASUREMENTS

Temitayo S. Adeyemi
Louisiana State University at Baton Rouge

INVESTIGATION OF GAS DYNAMICS IN WATER AND OIL-BASED MUDS USING DAS, DTS, AND DSS MEASUREMENTS

A Thesis

Submitted to the Graduate Faculty of the
Louisiana State University and
Agricultural and Mechanical College
in partial fulfillment of the
requirements for the degree of
Master of Science in Petroleum Engineering

in

The Craft and Hawkins Department of Petroleum Engineering

by
Temitayo Sheriff Adeyemi
B.S., University of Ibadan, Ibadan, 2019
May 2024

To my family in Nigeria, my best friend (Omotayo Juliana Oluwapelumi), and the world of people I've met in Louisiana.

Acknowledgments

I would like to thank ExxonMobil Research and Engineering Company and SwellFix LLC for providing funds to support this research. I also extend my gratitude to my collaborators who participated in this project: Sai Rao and V. Paul Gupta from ExxonMobil Upstream Research Company; Ganesh A. Samdani and Yashwant Moganaradjou from ExxonMobil Services & Technology Pvt. Ltd; Eric R. Upchurch from Chevron Technology Company; Michael Rolens, Nader Issa, and Albert Carmenate from Terra15; Yuanhang Chen, Otto Santos, Chen Wei, Mahendra Kunju, Mauricio Almeida, and Andreau Trepagnier from LSU. This author also appreciates the Society of Petroleum Engineers (SPE) Journal for the permission to reproduce some information contained in my previous publications.

Table of Contents

List of Tables

List of Figures

Abstract

Reliable prediction of gas migration velocity, void fraction, and length of gas-affected region in water and oil-based muds is essential for effective planning, control, and optimization of drilling operations. However, there is a gap in our understanding of gas behavior and dynamics in water and oil-based muds. This is a consequence of the use of experimental systems that are not representative of field-scale conditions. This study seeks to bridge the gap via the well-scale deployment of distributed fiber-optic sensors for real-time monitoring of gas behavior and dynamics in water and oil-based mud. The aforementioned parameters were estimated in real-time using optical fiber-based distributed acoustic sensor (DAS), distributed temperature sensor (DTS), and distributed strain sensor (DSS).

This is the first well-scale study conducted to investigate gas dynamics in oil-based muds using a variety of distributed fiber-optic sensors - DAS, DTS, and DSS. The gas migration velocity, void fraction, and length of the gas-affected region were estimated across the wellbore for a series of multiphase flow experiments carried out with gas injection (nitrogen and helium) in water and oil-based mud at various operating conditions. The results obtained using each of DAS, DTS, and DSS show good agreement with downhole gauges-based estimates and observations from surface gauges, validating the reliability of the distributed fiber-optic sensors for monitoring gas behavior and dynamics in water and oil-based muds.

Chapter 1. Introduction

1.1. Research motivation and relevance

Water- and oil-based muds are frequently employed in the oil and gas industry to serve various purposes during drilling and completion, such as formation pressure control, removal of cuttings, transmission of hydraulic power, and wellbore stability maintenance (Boyd et al. 1987). Due to its unique characteristics, the use of oil-based muds ensures higher lubricity, greater stability at high temperatures, and improved wellbore stability in shaly formations (Boyd et al. 1987). During drilling and completion operations, there is a tendency to encounter gas-bearing formations, leading to an unwanted fluid influx into the wellbore. Hence, a good understanding of gas influx dynamics in mud is essential, as this will impact the ability to implement effective and efficient well control measures. However, gas influx dynamics in oil-based muds, including the dynamic migration velocity, solubility effect, bottomhole pressure effect, and the change in gas void fraction as the gas migrates toward the surface are not fully understood. Currently, a discrepancy exists between the observed gas rise velocity in the field and the velocity estimate obtained via the industry-standard Taylor bubble correlations (Rader et al. 1975; Johnson et al. 1995; Jayah et al. 2013; Samdani et al. 2023a; Rao et al. 2022).

By investigating gas behavior in non-Newtonian fluids via laboratory experiments, computational fluid dynamics, and numerical simulations, attempts have been made by some authors to understand the origin of this discrepancy to develop a better model (Tariqul et al. 2019; Tariqul et al. 2022; Taotao et al. 2012; Hu et al. 2022; Li et al. 2002; Dewsbury et al. 1999). However, the fluids used (Xanthan solution and polymers) exhibit rheological properties that are quite different from those of drilling muds. This limits our ability to model and predict gas influx behavior accurately for better implementation of well control and kick removal operations.

Furthermore, only a few well-scale studies have been conducted to investigate gas influx dynamics (Feo et al. 2020; O'Brien 1981; Sharma et al. 2020; Santos et al. 2021; Casariego and Bourgoyne 1988; Samdani et al. 2023a), especially in oil-based muds (Samdani et al. 2023a). This is due to the limitation of not being able to create experimental setups that approximate well-scale conditions (Viana et al. 2003; Hasan and Kabir 1992; Rao et al. 2022). The well-scale study presented by Samdani et al. (2023a) was based on the use of downhole gauges, which limited their scope of investigation as the gas migration velocity could only be estimated at the locations of the downhole gauges.

The limitations of the previous studies therefore justify the need for a better and more accurate approach. Moreover, owing to the disparity in compositions and rheology properties, gas tends to behave differently in water and oil-based muds. This impacts the level of complexity of the measures required for effective well control while operating with either fluid. This is especially important where there is a possibility of penetrating gas-bearing formations. Studies have shown that gas-kick detection is more challenging in oil-based muds due to the solubility effect (Aboulrous et al. 2013; O'Brien 1981; Thomas et al. 1982; Anfinsin and Rommetveit 1992). When compared with water-based mud, gas-kick detection in oil-based mud is about three times slower due to the solubility effect (Leandro et al. 2014). This therefore necessitates a better understanding of gas dynamics and behavior in both water and oil-based muds at field-scale conditions for optimization of well control operations in the field.

1.2. Overview of distributed fiber-optic sensing

Distributed fiber-optic sensing is a surveillance technology that is rapidly gaining relevance in the oil and gas industry for real-time tracking of dynamic events in wellbores and reservoirs (Hartog 2017). DFOS operates on the principle of back-scattered light and is based on three

different mechanisms. These mechanisms are Rayleigh scattering, Raman scattering, and Brillouin scattering. Rayleigh scattering is an elastic scattering that is sensitive to dynamic strain, and it is typically used for distributed acoustic sensing. Raman scattering is an inelastic scattering that is sensitive to temperature, and it is commonly used for distributed temperature sensing (DTS). Brillouin scattering is an inelastic scattering that is sensitive to both strain and temperature, and it is typically used for distributed strain sensing (DSS). A typical fiber-optic consists of a glass core through which light pulse travels, a cladding that ensures total internal reflection, and a coating that protects it from environmental conditions (Figure 1). As shown in Figure 2, the back-scattered signals exhibit different wavelengths and intensities. DFOS overcomes one of the limitations of traditional point gauges by enabling a continuous measurement of strain rate and temperature in real-time across the whole length of the well at high resolutions in time and space, thereby making detailed monitoring of gas dynamics and behavior possible (Sharma et al. 2020).

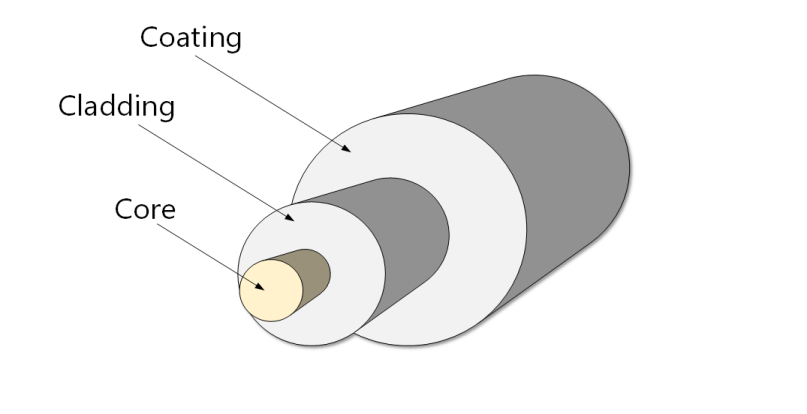

Figure 1. The basic components of an optical fiber (Ref: Cisco).

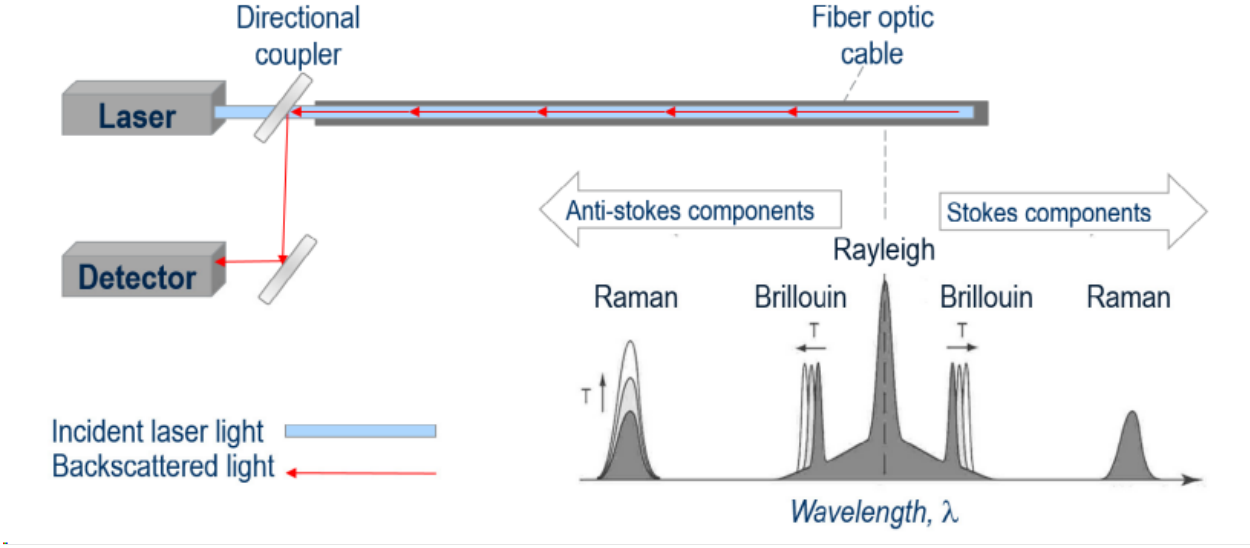

Figure 2. The backscattered light components for a fiber-optic system (Ekechukwu and Sharma 2023).

This study demonstrates the capability of DAS, DTS, and DSS for real-time monitoring and understanding of gas behavior and dynamics in water and oil-based muds. It is the first study conducted at a well-scale to investigate gas dynamics in oil-based mud using fiber-optic DAS, DSS, and DTS. This study seeks to shed some light on gas behavior in water and oil-based muds via well-scale experimental investigation and analysis. A series of gas-kick experiments were conducted in a 5163-ft wellbore instrumented with fiber-optic sensors. The fiber-optic DAS, DTS, and DSS data acquired were analyzed independently to estimate the gas migration velocity, length of gas-affected region, and gas void fraction. The results obtained using each of DAS, DTS, and DSS show excellent agreement with downhole measurements. The gas front and bottom velocity (FV and BV) estimates are also comparable with the predictions of commonly used multiphase flow correlations. Furthermore, the effects of gas influx rate and bottomhole pressure on gas dynamics in oil-based mud were investigated by analyzing well-scale tests conducted in oil-based mud at different bottomhole pressures and gas injection rates. The well-scale experiments also

highlight the effects of gas solubility as well as the rheology and composition of wellbore fluid on gas flow behavior and dynamics.

The subsequent chapters of this thesis are organized as follows: Chapter 2 highlights the objectives and novelties of this study as compared to previous studies in literature. The experimental setup and procedures employed for the fiber-optic data acquisition, processing, and interpretation, as well as flow correlations implementation, are described in Chapter 3. The results of the DAS, DTS, and DSS for the water and mud tests, comparison with the estimates from the numerical model, gauge analysis, and flow correlations, as well as the effects of bottomhole pressure, injection rate, and gas solubility on gas dynamics are discussed in Chapter 4. Finally, the key findings from the study as well as the suggested future directions are summarized in Chapter 5.

Chapter 2. Research Objectives and Novelties

2.1. Research objectives

The main objectives of this study are summarized below:

- Monitoring of gas injection, bullheading, and migration dynamics in water and oil-based muds using DAS, DTS, and DSS.
- Independent estimation of gas migration velocity, void fraction, length of the gas-affected region, and gas arrival time at the surface in water and oil-based muds using DAS, DTS, and DSS.
- Validation of fiber-optic results using surface and downhole gauges, numerical simulation, and existing multiphase flow correlations.
- Investigation of the effects of gas solubility, bottomhole pressure, and gas injection rate on gas behavior and dynamics in oil-based mud.

2.2. Previous studies and novelties

Attempts have been made by some authors to facilitate a better understanding of gas dynamics in water via well-scale studies of nitrogen gas behavior and dynamics in a water-filled wellbore using DAS, DTS, or a combination of both methods. To highlight the novelties of this study, a summary of previous well-scale studies is presented in Table 1**.** It is essential to bear in mind that most of the previous well-scale studies focused on the estimation and use of only gas migration velocity as a parameter for understanding gas behavior and dynamics. For instances where void fraction was estimated, the numerical modeling schemes employed could not accurately capture the initial conditions of the gas influx and some of the operational conditions (Wei et al. 2022; Wei and Chen 2022b; Santos et al. 2021. Furthermore, Samdani et al. (2023) conducted a well-scale study on nitrogen gas behavior in oil-based mud. However, this study was

limited to gas migration velocity estimation using downhole gauges. Reliable estimation of gas void fraction is important for proper planning and implementation of well control operations. It has been observed that pressure builds up in oil-based mud due to the gas solubility effect. This phenomenon was observed to persist until any entrained gas had completely dissolved in the mud. At this point, no further gas migration occurs. This increases the chances of a blowout occurrence when the entrained gas expands multiple times its original volume. On the other hand, pressure builds up continuously in water-based mud until the entrained gas reaches the surface (O'Brien 1981; Leandro et al. 2014). Due to the influence of void fraction on pressure dynamics during drilling and well control operations, reliable quantification of the gas void fraction is important for the effective and safe implantation of such operations. As discussed earlier, most of the previous well-scale studies did not explore void fraction dynamics and the results reported by a few of them were obtained via numerical schemes that did not accurately capture the operating conditions. Some experimental investigations that do not approximate field conditions have also been carried out (Nwaka et al. 2020; Pietrzak and Placzek 2019; Miyabayashi et al. 2022; Gopal 1998).

Table 1. Comparison of previous works with the current study

Reference	Wellbore Fluid(s)	Gas Monitoring with Fiber-Optic Sensor	Gas Migration Velocity			Gas Void Fraction	Gas Influx Length
		DAS	DTS	DSS	DAS		
Current Study	Water & Oil-based Muds	Yes	Yes	Yes	Yes	Yes	Yes
Feo et al. (2020)	Water	Yes	Yes	No	Yes	No	No
Santos et al. (2023)	Water	Yes	No	No	Yes	No	No
Sharma et al. (2021)	Water	Yes	No	No	Yes	No	No
Sharma et al. (2020)	Water	Yes	Yes	No	Yes	No	No
Santos et al. (2021)	Water	Yes	No	No	Yes	Yes	No
Samdani et al. (2023)	Oil-based Mud	Yes	No	No	Yes	No	No
Jagadeeshwar et al. (2023)	Water	Yes	Yes	No	Yes	No	No
Wei and Chen (2022b)	Water - based Mud	No	No	No	No	Yes	No
Wei et al. (2022)	Water - based Mud	No	No	No	No	Yes	No
Williams et al. (2020)	Water	Yes	Yes	No	Yes	No	No

The limitations of the previous studies justify the need for a better and more accurate approach to monitoring and understanding gas behavior and dynamics in water and oil-based muds. This study demonstrates the capability of DAS, DTS, and DSS for real-time monitoring and understanding of gas behavior and dynamics in water and oil-based muds. It is the first well-scale investigation of gas dynamics in oil-based mud with solids using distributed fiber-optic measurements. The study seeks to shed some light on gas behavior in water and oil-based muds via well-scale experimental investigation and analysis.

As discussed in the previous chapter, the DSS surveillance technology employs the mechanism of an inelastic light scattering that is sensitive to both temperature and strain. The technology has been employed in literature for monitoring static strain and assessing the integrity of structures (Zhang et al. 2010; Sasaki et al. 2019; Zhang et al. 2021; Sang et al. 2019; Kogure and Okuda 2018; Yoshida et al. 2002; Blanc et al. 2022; Baldwin 2015; Zhang and Xue 2019). It was also deployed by Ugueto (2021) to monitor hydraulic fracturing in unconventional reservoirs, but the work was limited to intermittent strain measurement. Therefore, this study is also the first exploration of the applicability of DSS for monitoring dynamic, fast-changing events like gas behavior in oil-based mud at the well-scale.

Chapter 3. Methodology

3.1. Experimental set-up and procedure

The sets of experiments analyzed in this work were carried out at the Petroleum Engineering Research, Training, and Testing (PERTT) lab facility located at the Louisiana State University (LSU) campus. Figure 3a shows the geographical location of the PERTT lab facility where the experiments were conducted. The PERTT facility consists of several equipment and subsurface structures suitable for field-scale investigation of multiphase flow phenomena. These include field-scale wells, fluid circulation systems, surface and downhole flow monitoring devices, and an underground gas storage system. A detailed description of the PERTT facility is presented in Sharma et al. 2020. A schematic of the test well in which the analyzed experiments were conducted is shown in Figure 3b. The test wellbore of depth 5800 ft consists of a bridge plug (set at 5163 ft) and a tubing of length 5025 ft on which single-mode and multimode fibers are clamped. The DAS measurements were obtained via the single-mode fiber, while the multimode optical fiber was employed for the DSS and DTS measurements. Also installed in the wellbore are four downhole pressure and temperature gauges A, B, C, and D. These gauges are located at depths of 487 ft, 2023 ft, 3502 ft, and 5024 ft respectively. A chemical injection line (half-inch in diameter) used for some of the experiments conducted at low injection rates is also attached to the tubing. This is shown in Figure 3b.

Tests 1 to 5 were analyzed to monitor and characterize gas migration in oil-based mud. The effects of gas injection rate and bottomhole pressure on gas migration velocity in oil-based mud were investigated. Table 2 summarizes the specifications of the DAS and DTS data acquisition for Tests 1 to 5. Experiments 6 and 7 were analyzed to compare gas signatures and void fraction in water and oil-based muds. Table 3 summarizes the specifications of the DAS, DSS, and DTS data

acquisition for Tests 6 and 7. Tests 8 and 9 were conducted to investigate the effect of gas solubility on gas behavior and dynamics in oil-based mud. Table 4 summarizes the DAS acquisition parameters for Tests 8 and 9.

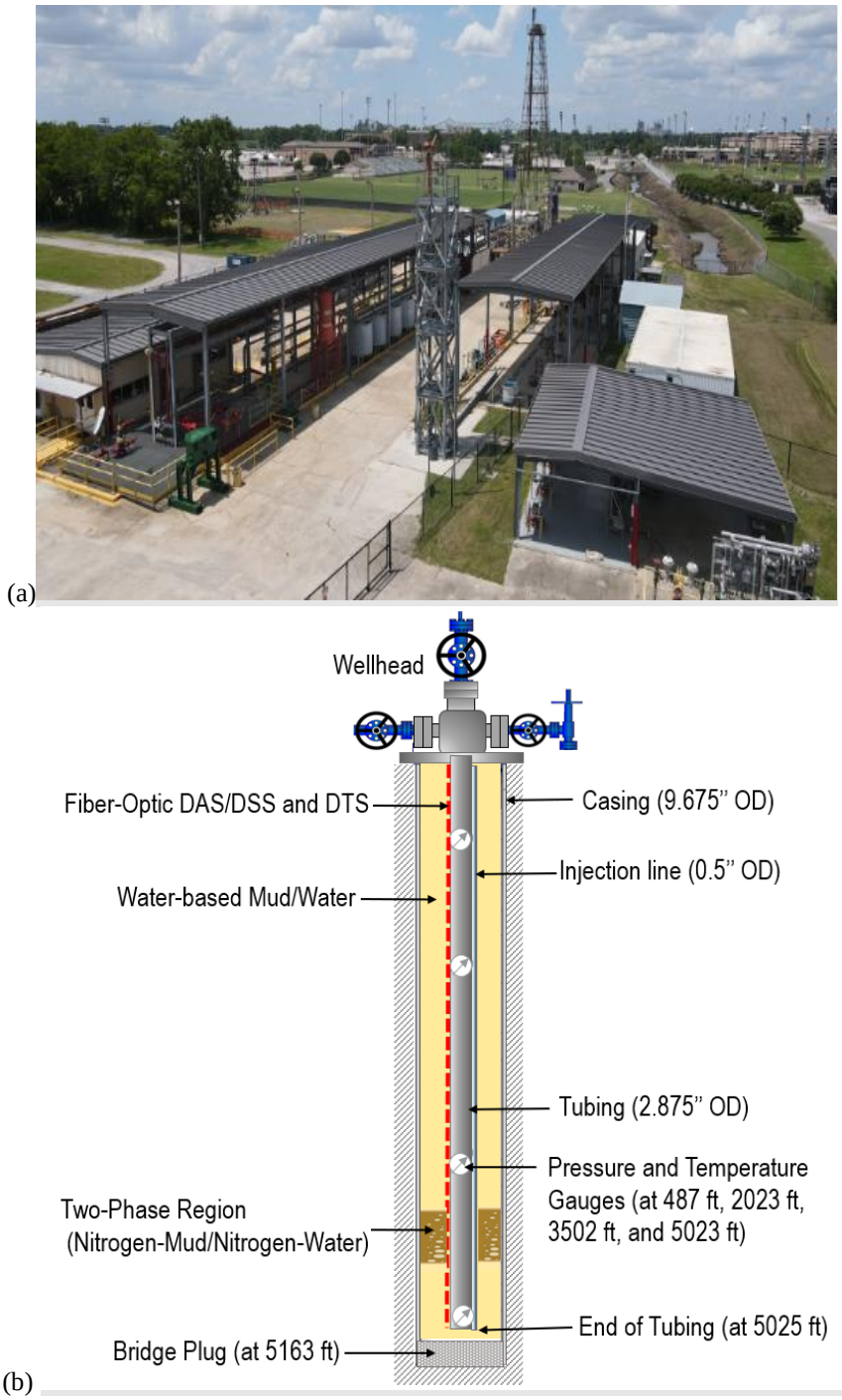

Figure 3. (a) LSU PERTT lab facility (b) schematic of the test well (Adeyemi et al. 2023b)

Table 2. DAS and DTS measurement specification for Tests 1 to 5 (Adeyemi et al. 2023b)

DTS		**DAS**	
Optical mode	Multimode	Optical mode	Single-mode
Spatial resolution	3.28 ft	Spatial resolution	6.53 ft
Sampling interval	1.64 ft	Sampling interval	2.45 ft
Temporal resolution	10 sec	Temporal resolution	0.00025 sec
Range	15 km	Range	16 km
Accuracy	±0.9 °F	Frequency	4 kHz
Operating Temperature	32 to 122 °F	Gauge Length	6.53 ft

Table 3. DAS, DTS, and DSS measurement specification for Tests 6 and 7 (Adeyemi et al. 2023b)

DTS		**DSS**		**DAS**	
Optical mode	Multimode	Optical mode	Multimode	Optical mode	Single-mode
Spatial resolution	3.28 ft	Spatial resolution	32.8 ft	Spatial resolution	6.53 ft (Test 6) and 19.69 ft (Test 7)
Sampling interval	1.64 ft	Sampling interval	0.33 ft	Sampling interval	2.45 ft (Test 6) and 6.54 ft (Test 7)
Temporal resolution	10 sec	Temporal resolution	40 sec	Temporal resolution	10^{-4} sec (Test 6) and 10^{-3} sec (Test 7)
Range	15 km	Range	60 km	Range	16 km
Accuracy	±0.9 °F	Accuracy	±0.5 °F	Frequency	10 kHz (Test 6) and 1 kHz (Test 7)
Temperature Range	32 to 122 °F	Temperature Range	-13 to 176 °F	Gauge Length	6.53 ft and 19.69 ft

Table 4. DAS acquisition parameters for Tests 8 and 9.

Optical mode	Single-mode
Spatial resolution	6.53 ft
Sampling interval	2.45 ft
Temporal resolution	0.025 sec
Range	16 km
Frequency	40 Hz
Gauge Length	6.53 ft

The test well was filled with synthetic-based mud (or water). The synthetic-based mud (SBM) used in this study has a density of 8.34 ppg, yield point of 16 lb./100ft^2, and plastic viscosity of 15 cP. The interfacial tension between nitrogen gas and the SBM used in this study ranges between 21.2 dyne/cm and 7.9 dyne/cm, for a pressure range of 800 to 3600 psi (Samdani et al. 2023a). Also, the percentage by volume of low and high-gravity solids in the SBM are 2.6% and 9.7% respectively. The properties of the SBM utilized in this study are summarized in Table 5 below.

Table 5. Properties of the SBM utilized in this study (Adeyemi et al. 2023b).

Mud Density (lb./ft^3)	**Plastic Viscosity (cP)**	**Yield Point (lb. /100ft^2)**	**Interfacial Tension (dyne/cm)**	**Low-gravity Solids (%)**	**High-gravity Solids (%)**
62.4	16-21	16	17.9 - 21.2 [800 – 3600 psi]	2.6	9.7

A summary of the experiments analyzed in this study is presented in Table 6**.** The test matrix presented in Table 6 is a superset of the test matrix presented in Samdani et al. (2023a). A similar test number nomenclature was used for ease of reference, especially during the comparison of the fiber-optic results with the gauges-based results presented in Samdani et al. (2023a).

Experiments 1 to 5 involved the injection of a fixed amount of nitrogen gas through the tubing (or the half-inch chemical injection line) while maintaining the desired bottom-hole pressure. During gas injection, mud was displaced and removed from the top of the annulus. Monitoring of the migration of the injected gas in real-time was carried out via DAS, DTS, downhole, and surface gauges. Experiments 6 and 7 involved the injection of gas through the tubing and then bullheading the gas down the tubing by circulating water (or mud), while maintaining the desired backpressure and taking returns through the annulus. Distributed fiber-optic sensor (DAS, DTS or DSS), downhole, and surface gauges were then employed for real-time monitoring of the gas migration.

Table 6. Well-scale tests matrix for the experiments analyzed in this study.

Test #	Fiber-Optic Data	Injected Volume (bbl.)	Injection Method	Test Type	Bullheading Rate (gpm)	Gas Type	Wellbore Fluid Type	Injection Rate (bpm)	Bottom-hole Pressure (psi)
1	DAS and DTS	20.0	Tubing	Migration	250	Nitrogen	Oil-based mud	6	3600
3	DAS and DTS	20.0	Injection line	Migration	-	Nitrogen	Oil-based mud	0.25	2290
4	DAS and DTS	20.0	Tubing	Migration	250	Nitrogen	Oil-based mud	6	2290
5	DAS and DTS	20.0	Tubing	Migration	200	Nitrogen	Oil-based mud	4.5	4500
6	DAS and DTS	8.0	Tubing	Circulation	200	Nitrogen	Water	-	-
7	DAS and DSS	8.4	Tubing	Circulation	200	Nitrogen	Oil-based mud	-	-
8	DAS	5.0	Tubing	Migration	250	Nitrogen	Oil-based mud	-	-
9	DAS	5.0	Tubing	Migration	250	Helium	Oil-based mud	-	-

For Tests 1 to 5, the DAS and DTS measurements were used to independently estimate the gas migration velocity. For Tests 6 and 7, gas front, and rear velocities, length of gas-affected region, and gas void fraction were estimated independently using DAS and DTS (or DSS).

Before discussing the methodology employed for the analysis and interpretation of the acquired DAS and DTS data, I think it is necessary to comment on the uncertainty level in the fiber-optic measurements. A detailed analysis of the error and uncertainty associated with the DTS and DAS measurements has been carried out by Wei et al. (2023b) to ascertain the degree of accuracy, comparability, and reliability of the DAS and DTS measurements. By calibrating the DTS data with a reference coil on the surface, the DTS temperature resolution was found to be 0.2 ℉ or 0.11 ℃ with the averaged calibration error of $\pm$ 1.8 ℉ ($\pm$ 1.0 ℃). The uncertainty in the DAS measurement depends on the noise floor of the optoelectronic data acquisition unit, which also depends on the acquisition parameters. For the DAS system used in this study, a maximum of 10% uncertainty can be expected from the DAS results (Wei et al. 2023b). The low level of uncertainty reinforces my confidence in the DAS and DTS results presented in the subsequent chapters of this thesis.

3.2. Fiber-optic data processing

The signal processing techniques implemented on the DAS, DSS, and DTS data to enhance the quality and visibility of the gas signature are described in this section. Implementation of the signal processing techniques is essential for accurate quantification of the parameters used to describe gas dynamics in water and oil-based muds. The fiber-optic data acquired from the wellbore are inherently noisy. The sources of the noise include fiber slippage, pump vibration, laser noise, noise introduced due to local oscillation, and digitization of the backscatter signals. Signal noise cannot be avoided, and different fiber-optic interrogators have different noise

threshold levels (as evident in the data acquired in this study using different interrogators). This therefore necessitates the implementation of some signal processing techniques on the DAS, DTS, and DSS data to enhance the visibility of the gas signature and improve gas-kick detection.

3.2.1. Analysis of the DAS data

The DAS (acquired in .hdf5 or .segy format) is a representation of the spatiotemporal strain rate data obtained in real-time from the wellbore. Figure 4 shows that the gas signature is not so visible from the DAS strain rate measurements. Hence, rigorous processing of the acquired DAS strain rate data is required to understand the gas behavior and dynamics. The first step in processing the DAS data involves the implementation of frequency band energy (FBE) analysis (Sharma et al. 2021; Jagadeeshwar et al. 2023). The FBE analysis minimizes the background noise effects for the best-performing frequency band. The best-performing frequency band refers to the frequency band that is least sensitive to background noise and best captures gas flow dynamics. It is, therefore, most suitable for both quantitative and qualitative description of gas dynamics in the wellbore. This frequency band was identified via spectrum analysis (Figure 5). The result of the spectrum analysis (Figure 5) shows that the 10 – 50 Hz frequency band best describes the gas migration dynamics. To implement the FBE techniques, the DAS strain rate data was partitioned into equal time windows, and fast Fourier transform (FFT) was applied to each time window to convert the DAS strain rate data from the time domain to the frequency domain. The algorithm returns the signal energy summed over some pre-defined frequency intervals and then concatenates the output for all the time windows. In addition to background noise minimization, the FBE also serves as a powerful technique for reducing the size of the acquired DAS data via intelligent compression that preserves signal quality. This helped to overcome the computational challenges associated with the handling of the DAS datasets of massive sizes. For instance, the DAS data obtained in this

study was about 2.0 Gb for every 10 seconds and the FBE method was employed to reduce it to about 1.0 Mb for every 10 seconds. Thereby, overcoming a major hurdle associated with data handling.

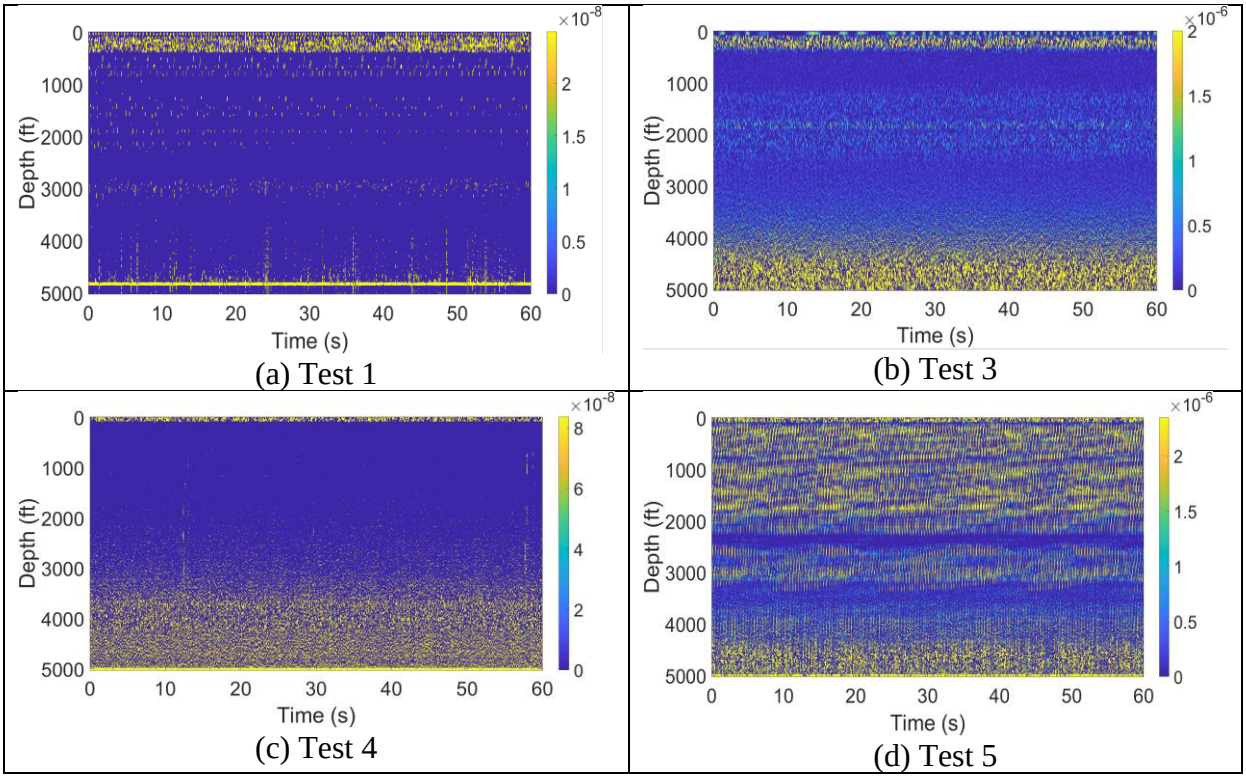

Figure 4. DAS strain rate waterfall plots for Tests 1 to 5 (Adeyemi et al. 2023a).

After the implementation of the FBE techniques, observation shows that the gas signature was still not visible for some of the tests. This is especially evident in Figure 6a where the gas migration signature during Test 6 could not be seen. This is probably due to the type of interrogator employed for that particular test. This therefore necessitates further processing. Consequently, a combination of additional signal denoising tools like a higher-order gradient filter, gradient-based iterative destroying algorithm, and Gaussian filter (Bouali 2010; Jagadeeshwar and Sharma 2023; Haddad and Akansu 1991; Stefano 2008) was employed to improve the gas signature visibility by reducing the effects of high-frequency background noise.

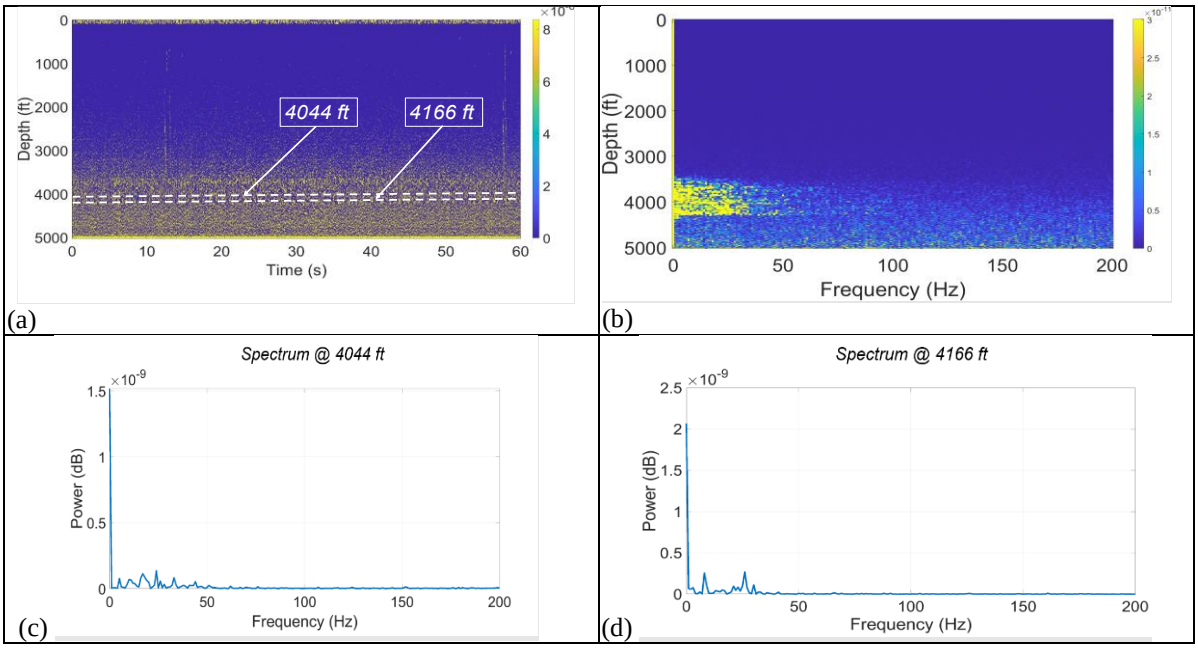

Figure 5. (a) An example of DAS strain-rate data acquired during Test 4 which shows gas below 3500 ft depth (b) 2D DAS spectrum (c-d) DAS spectrums at different depths to identify the best-performing frequency band (Adeyemi et al. 2023a).

A detailed mathematical description of the application of each of the aforementioned signal-denoising tools to fiber-optic data processing is presented in Jagadeeshwar and Sharma (2023). As evident in Figure 6b, the gas migration signature becomes visible after the implementation of the additional signal-denoising methods. This makes the front and bottom gas rise velocities, as well as the length of the gas-affected region trackable.

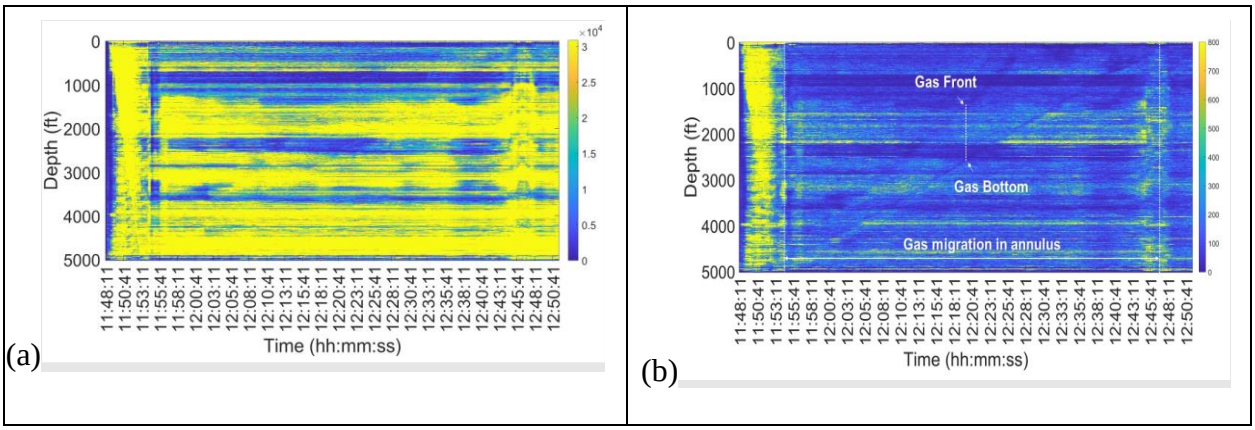

Figure 6. DAS result for nitrogen in water in Test 6 (a) FBE [10-50 Hz] waterfall (b)FBE [10-50 Hz] after additional signal denoising (Adeyemi et al. 2023b).

In an attempt to improve the visibility of the gas injection signature for Tests 1 to 5, the DAS strain rate data was also processed and analyzed in the low-frequency range (0 – 0.03 Hz). The low-frequency range consideration was necessitated by the lack of visibility of the gas injection signature on the high-frequency DAS. Low-frequency DAS is sensitive to both strain and temperature effects (Ekechukwu and Sharma 2021) and it has been found great usefulness in pressure estimation, gas signature detection, and hydraulic fracture characterization (Chen 2021; Jin and Roy 2017; Haavik 2022; Sharma et al. 2020). A detailed description of the use of low-frequency DAS for improving the quality of gas signatures is presented by Sharma et al. 2020.

3.2.2. Analysis of the DSS data

The Brillouin-based DSS is sensitive to both temperature and strain effects. To understand the overall effect of the gas dynamics on the DSS, the strain and temperature effects were not decoupled. Hence, the analyzed DSS data bears the imprints of both effects. The DSS data was acquired in .h5 file format. A visualization of the DSS data acquired during Test 7 (Figure 7a) does not show a very clear signature of the gas. This is due to the low quality of the DSS data. The low data quality is attributable to the loose tube configuration and data acquisition on multimode fiber.

To improve gas detection using DSS, additional signal processing methods were implemented on the acquired DSS data. The result obtained after the implementation of gradient filtering with respect to time is shown in Figure 7b**.** Although Figure 7b shows some improvement, the signal was still affected by some background noise. Convolution filtering was therefore employed to further improve the signal quality. Convolution filtering is a commonly used method in computer vision for image edge detection and quality enhancement (Haddad and Akansu 991; Stefano 2008) described mathematically by Equation (1) below.

$$G(x,y) = \omega * F(x,y) = \sum_{dx=-a}^{a} \sum_{dy=-b}^{b} \omega(dx,dy) F(x+dx, y+dy) \quad (1)$$

Where $G(x,y)$ is the output signal, ω is the convolution filter, $F(x,y)$ is the input signal, $dx\ and\ dy$ are the horizontal and vertical strides, respectively. As shown in Figure 7c, a notable improvement was observed. The processed DSS data was then used to estimate the front and rear velocities of the gas, gas void fraction, and the length of the gas-affected regions.

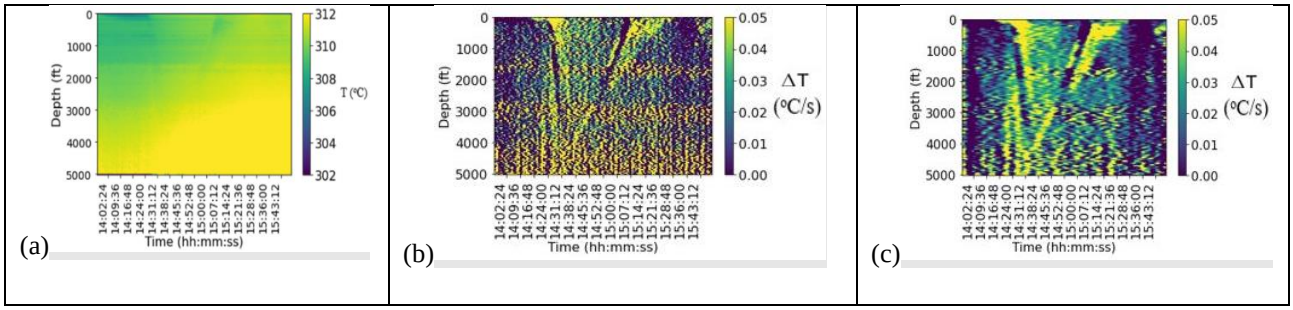

Figure 7. DSS results for nitrogen in mud in Test 7 (a) Unprocessed DSS (b) DSS gradient (c) DSS gradient after convolution filtering (Adeyemi et al. 2023b).

3.2.3. Analysis of the DTS data

DTS data was also acquired for the conducted experiments (except Test 7 where DSS was acquired). A spatiotemporal waterfall plot of the DTS temperature shows that the data was also affected by background noise and therefore requires some processing. As shown in Figure 8, the gas signature could be seen after implementing gradient filtering with respect to time. However, the gas signature was still very much buried in the background noise. Hence, the convolution filtering described in the previous section was also implemented on the DTS data. Different kernel sizes were used and remarkable improvement in signal quality was observed, as the gas signatures are clearly visible (Figure 9).

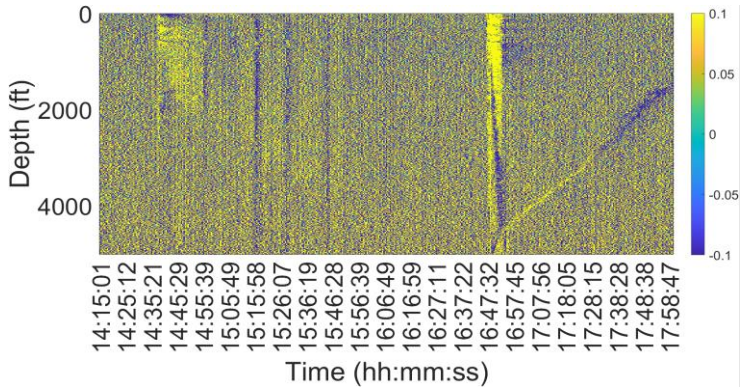

Figure 8. DTS gradient for Test 1 without any processing (Adeyemi et al. 2023a).

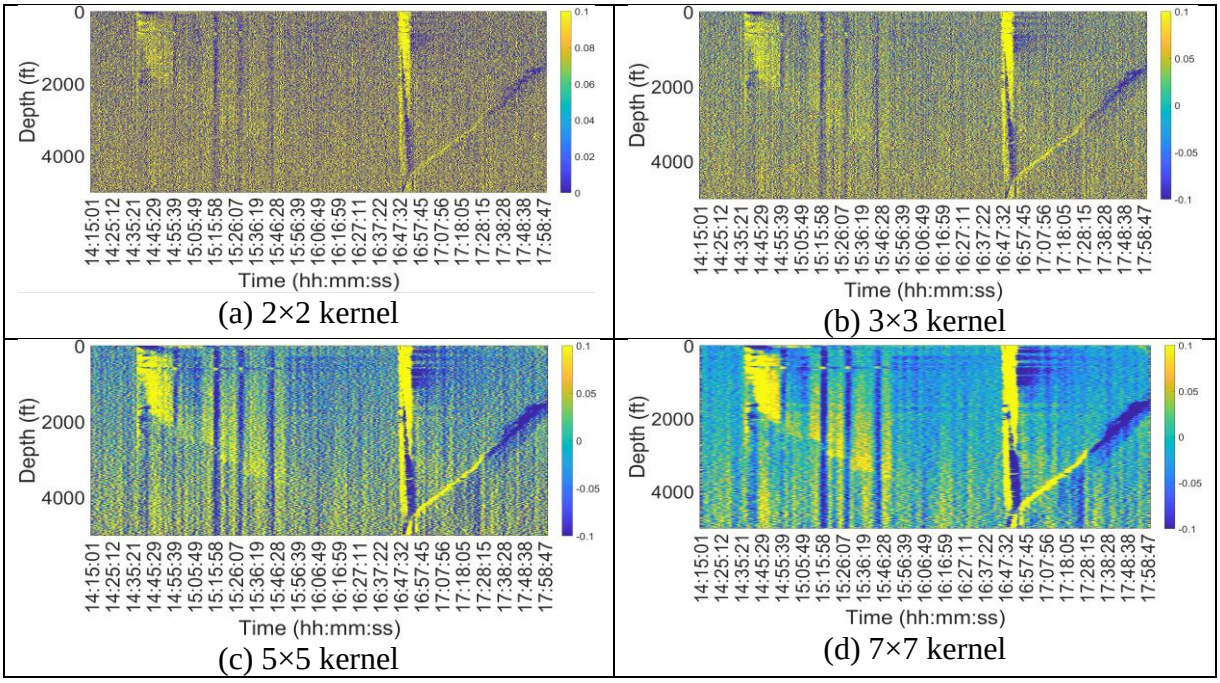

Figure 9. A convolution filter implemented on DTS data for Test 1 using different kernel sizes (Adeyemi et al. 2023a).

3.2.4. Gas Rise Velocity Estimation

To estimate the front and rear velocities of the gas between the gauges, which are important parameters of interest for this study, the F-K transform was implemented on both the processed DAS and DTS data (Sharma et al, 2020) for independent velocity estimations at different depths. FFT was applied to both time and space dimensions to obtain frequency and wave-number domains, respectively. F-K transform is a tool commonly used in processing seismic signals to reduce the effect of propagation noise (Kim, Cho, and Yi 2007). This involves the application of

2D FFT to a spatial-temporal matrix to obtain a new matrix in the F-K domain. The front and bottom velocities of the gas in the annulus were computed as the slope of the F-K transform, as the gas crossed the different gauge locations. A detailed mathematical description of the use of the F-K transform for gas rise velocity estimation is presented by Sharma et al. (2020).

3.2.5. Void fraction estimation

This section describes the methodology employed for gas void fraction estimation. The instantaneous void fraction estimation is illustrated schematically in Figure 10 using the scenario when the migrating gas was between downhole gauges B and C. Void fraction estimation requires that the instantaneous pressure-drop (estimated from the downhole gauges) and the length of the two-phase gas-liquid region (estimated from the fiber-optic data) be known. For the scenario illustrated in Figure 10, the pressure-drop (Δp) *between* gauges B and C at the instance when the bottom of the gas crosses gauge C (around 14:46:35) is about 53.3 and the length of the two-phase gas-liquid region (h) at that instance is about 344 ft. The instantaneous gas void fraction was then estimated using the equation (2) below.

$$Gas\ Fraction = \frac{\Delta P}{0.052 \times (\rho_l - \rho_g) \times h} \qquad (2)$$

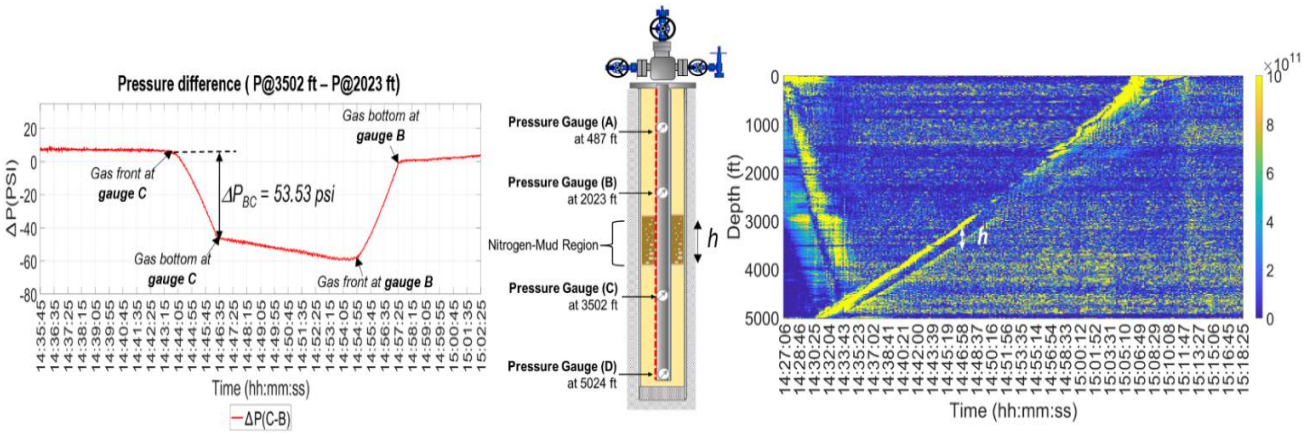

Figure 10. Estimation of void fraction from fiber-optic and pressure drop data (Adeyemi et al. 2023b).

3.3. Results validation approach

Three different methods were employed in this study to ascertain the reliability of the DAS, DTS, and DSS results. The first approach involves the use of downhole gauges. The downhole gauges were employed to estimate the front and rear velocities of the gas. The velocity estimates obtained using the downhole gauges were then compared with DAS, DTS, and DSS predictions. The comparison shows good agreement between the downhole gauges and the fiber-optic sensors.

The use of downhole gauges for gas rise velocity estimation and real-time tracking of instantaneous gas locations is illustrated in Figure 11. Gas entry into the region between the downhole gauges is indicated by the decrease in the hydrostatic pressure in the region. The hydrostatic pressure decline is due to the reduction in the average fluid density in the annular region between the gauges. This phenomenon is illustrated schematically in Figure 11a, using the downhole gauge data acquired during Test 1**.** The time t_1 represents the instance when the front of the gas crossed gauge C. It is confirmed by the onset of continuous decline in the hydrostatic pressure difference between the downhole gauges B and C (ΔP_{C-B}), as illustrated in Figure 11b. A minimum pressure difference was observed at time t_2, indicating the instance when the gas bottom crossed gauge C. Conversely, at time t_3, when the front of the gas crossed downhole gauge B, an increase in ΔP_{C-B} was observed due to an increase in the average fluid density in the region as some part of gas had left the region. It marked the onset of a continuous increase in ΔP_{C-B} until all the gas had left the region between gauges C and B. Finally, time t_4 represents the instance when the gas bottom crossed gauge B and at that instance, the absolute value of ΔP_{C-B} is minimum. This is an expected observation as the average fluid density is maximum when there is no gas in the annular region between the downhole gauges C and B. The understanding of the instantaneous

locations of the front and bottom of the gas was combined with the knowledge of the gauge locations to obtain the gauges-based FV and BV estimates presented in Table 16.

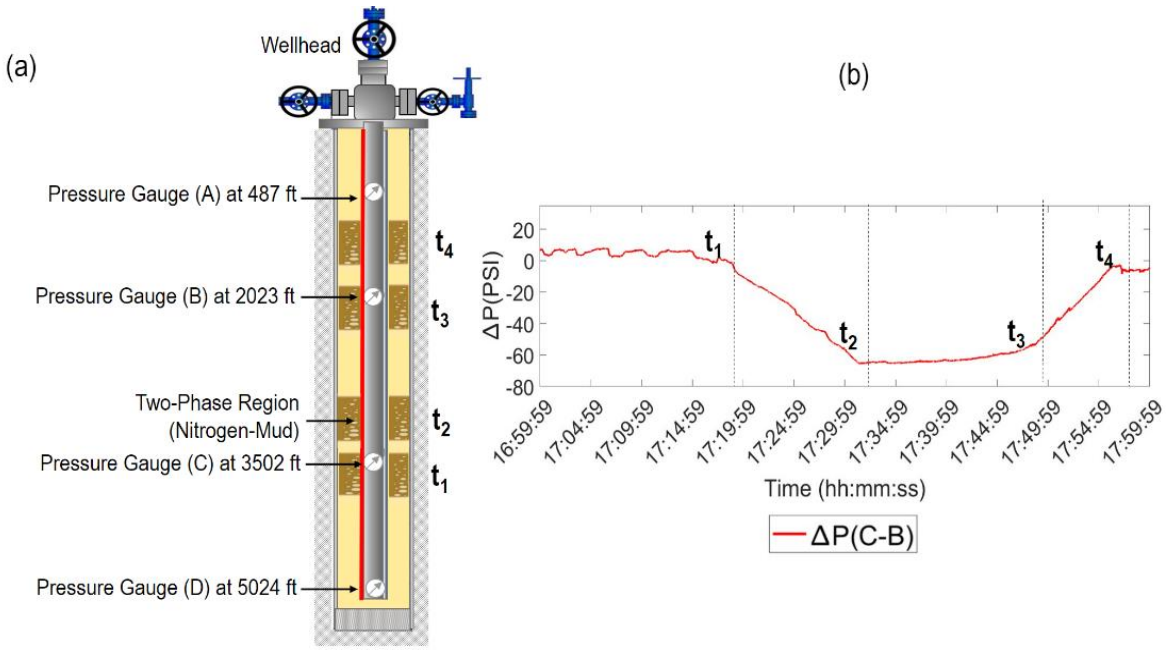

Figure 11. Description of gas migration dynamics during Test 1 using downhole gauges (Adeyemi et al. 2023a).

The fiber-optic result was also compared with the predictions obtained using four commonly used multiphase flow correlations for gas migration velocity. These correlations are summarized in Table 7.

The comparison shows reasonable agreement between the fiber-optic result and some of the multiphase flow correlations. Finally, the gas rise velocity and void fraction estimates obtained independently using DAS, DTS, and DSS were also compared with the results obtained via numerical simulation (Chen et al. 2023). The comparison shows good agreement between the fiber-optic and numerical simulation results.

Table 7. Flow correlations used for comparing gas rise velocity in the annulus (Adeyemi et al. 2023b).

Flow Correlation	**Equation**
Harmathy (1960)	$u = 0.4774\left(\frac{\sigma(\rho_l - \rho_g)}{{\rho_l}^2}\right)^{0.25}$
Zuber and Hench (1962)	$u = 0.4774\left(\frac{\sigma(\rho_l - \rho_g)}{{\rho_l}^2}\right)^{0.25} H^{0.5}$
Griffith and Wallis (1961)	$u = 1.637 \times K\left(\frac{D_2(\rho_l - \rho_g)}{\rho_l}\right)^{0.5}$
Griffith (1964)	$u = 1.637 \times K\left(\left(\frac{D_2 - D_1}{2}\right)\left(\frac{\rho_l - \rho_g}{\rho_l}\right)\right)^{0.5}$
$K = 0.345 - 0.037\left(\frac{D_1}{D_2}\right) + 0.235\left(\frac{D_1}{D_2}\right)^2 - 0.134\left(\frac{D_1}{D_2}\right)^3$	

Surface gauges were also employed to monitor gas dynamics and validate fiber-optic results. The duration of major events such as gas injection, bullheading, and gas migration were estimated from the surface gauges. Gas injection period is indicated on the surface gauges by continuous decrease in the storage wells pressures. The entry of the injected gas into the annulus is indicated by an increase in casing pressure and a sudden rise in the casing pressure is observed at the instance the gas arrived at the surface. Observations from the surface gauges show good agreement with the results obtained from the fiber-optic sensors. The results of the surface gauges analysis for Tests 1 to 5 are presented in Chapter 4.

Chapter 4. Results and Discussions

This chapter discusses the results of the water and mud tests conducted in this study. These experiments are summarized in Table 8. Tests 1 to 5 were conducted to understand gas dynamics in oil-based mud using fiber-optic sensors, and also investigate the effects of bottomhole pressure and gas injection rate on gas behavior and dynamics in oil-based mud. Tests 6 and 7 were conducted to understand the effect of rheology on gas behavior and dynamics. Two additional experiments (Tests 8 and 9) were also conducted using different gases (helium and nitrogen) to gain insight into the effect of gas solubility on gas dynamics in oil-based mud. The fiber-optic, surface gauges, and downhole gauges data acquired during the experiments were processed and analyzed. The results obtained and their implications on gas behavior and dynamics are thoroughly discussed in this chapter.

Table 8. Summary of the water and mud tests analyzed in this study.

Test #	Injected Volume (bbl.)	Injection Method	Test Type	Bullheading Rate (gpm)	Well-bore Fluid Type	Injected Gas Type
1	20.0	Tubing	Migration	250	Oil-based mud	Nitrogen
3	20.0	Injection line	Migration	-	Oil-based mud	Nitrogen
4	20.0	Tubing	Migration	250	Oil-based mud	Nitrogen
5	20.0	Tubing	Migration	200	Oil-based mud	Nitrogen
6	8.0	Tubing	Circulation	200	Water	Nitrogen
7	8.4	Tubing	Circulation	200	Oil-based mud	Nitrogen
8	5.0	Tubing	Migration	250	Oil-based mud	Nitrogen
9	5.0	Tubing	Migration	250	Oil-based mud	Helium

4.1. Fiber-optic results for gas migration in water

The results of the DAS and DTS analysis for Test 6 are presented in this section. The signal processing techniques discussed in Chapter 3 were implemented on the fiber-optic data to enhance the visibility of the gas signatures. The gas signatures during the water test are most visible in the 10 – 50 Hz frequency range. Consequently, the FBE corresponding to the 10 – 50 Hz frequency range was selected for further analysis and interpretation. The processed DAS FBE plot for the 10 – 50 Hz frequency band is shown in Figure 12a. The gas signatures that were initially buried in the background noise are clearly visible after implementing the signal processing techniques discussed in Chapter 3 (Figure 12a). Similarly, the visibility of the gas migration signatures was greatly enhanced after the implementation of additional signal processing techniques on the DTS data (Figure 12b).

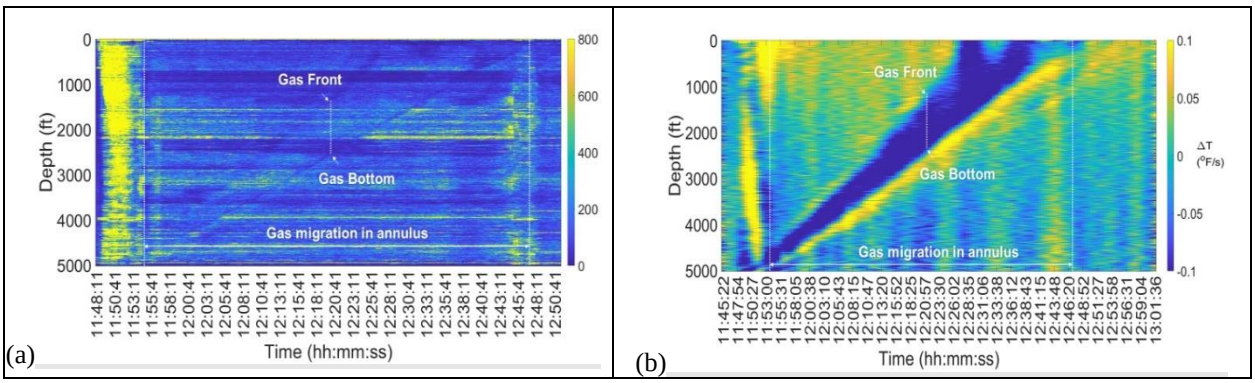

Figure 12. Waterfall plots for Test 6 (nitrogen in water) (a) Processed DAS FBE (b) DTS gradient (Adeyemi et al. 2023b).

As discussed in Chapter 3, the gas rise velocity was obtained from the fiber-optic data via F-K analysis. The front and bottom velocity (FV and BV, respectively) estimates were obtained at instances when the gas crossed the downhole gauges to facilitate results validation via comparison with gauges-based results. The results of the F-K implementation on the DTS data are shown in Figure 13. The estimation of the FV and BV from the F-K signatures is illustrated in Figure 13a.

For instances where the F-K signatures were not very visible, the FV and BV were estimated manually from the waterfall plots of the processed DAS and DTS data.

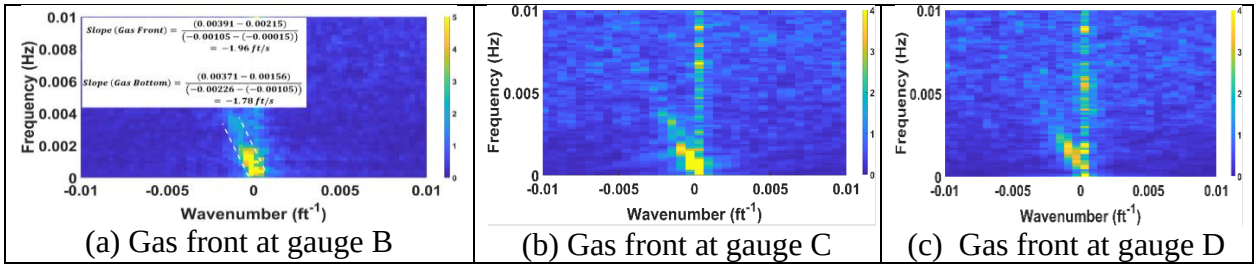

(a) Gas front at gauge B (b) Gas front at gauge C (c) Gas front at gauge D

Figure 13. F-K transforms at different depths implemented on the DTS data for Test 6 (Adeyemi et al. 2023b).

As discussed earlier, the FV and BV of the gas were also estimated using the downhole gauges. This was done to facilitate the validation of the fiber-optic results. The pressure gauge data for the water test is shown in Figure 14 below. Figure 14 was used to estimate the times and pressure drops when the front and bottom of the gas crossed each of the downhole gauges. The information was then combined with the knowledge of the gauge locations to estimate the average void fraction, as well as the average FV and BV at different gauge locations. The results obtained are summarized in Table 9.

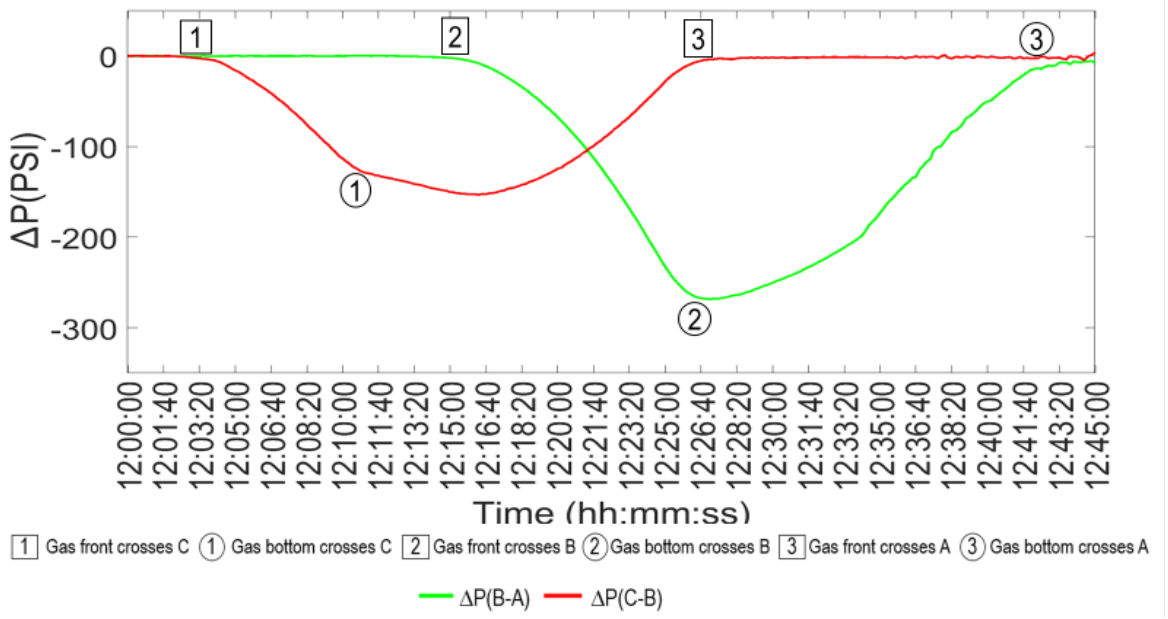

Figure 14. Gas front and bottom locations and observed pressure drop trends during Test 6 (Adeyemi et al. 2023b).

Table 9. Gauges-based velocities for Test 6 (Adeyemi et al. 2023b).

	Time	**FV (ft/s)**		**Time**	**BV (ft/s)**		**Pressure Drop (psi)**
Gas front at gauge C	12:04:50	1.81	Gas bottom at gauge C	12:11:20	1.64	ΔP_{CB}	126.69
Gas front at gauge B	12:15:40	2.09	Gas bottom at gauge B	12:26:50	1.76	ΔP_{BA}	254.40
Gas front at gauge A	12:26:50	2.18	Gas bottom at gauge A	12:41:20	1.83	ΔP_{DC}	97.37

Table 10 shows the existence of good agreement between the velocity and void fraction estimates obtained independently using DAS and DTS, as well as with the gauges-based results presented in Table 9. The fiber-optic results also show reasonable agreement with some of the existing multiphase flow correlations (Table 11). This shows the reliability of the fiber-optic sensors for monitoring gas behavior and dynamics. It is also observable from Table 10 that both the gas void fraction and length of the gas-affected region increase from the bottom of the wellbore to the surface. This is due to the effect of lower gas solubility at lower pressure near the surface.

Table 10. DAS and DTS results for Test 6 (Adeyemi et al. 2023b).

Time	**Event**	**DAS**			**DTS**			Gas Void Fraction
		FV (ft/s)	BV (ft/s)	Gas Region Length (ft)	FV (ft/s)	BV (ft/s)	Gas Region Length (ft)	
12:04:50	Gas front at gauge C	1.87	1.69	502	1.85	1.70	508	0.43
12:15:40	Gas front at gauge B	2.04	1.73	750	1.96	1.78	738	0.47
12:26:50	Gas front at gauge A	2.10	1.77	923	2.14	1.84	927	0.52

Table 11. Estimated gas rise velocity for Test 6 using DAS, DTS, and flow correlations (Adeyemi et al. 2023b).

Time	Event	Average Gas Migration Velocity (ft/s)					
		DAS	DTS	Bubble flow (Griffith 1964)	Bubble flow (Harmathy 1960)	Bubble flow (Zuber and Hench 1962)	Slug flow (Griffith and Wallis 1961)
12:04:50	Gas front at Bank C	1.87	1.85	2.13	2.00	1.72	2.80
12:15:40	Gas front at Bank B	2.04	1.96	2.16	2.01	1.73	2.84
12:26:50	Gas front at Bank A	2.10	2.14	2.18	2.02	1.73	2.88
Water-Nitrogen Interfacial Tension (σ) = 70 dyne/cm, Water Density (ρ_l) = 8.33 ppg, Annular Geometry Factor (K) = 0.354							

4.2. Fiber-optic results for gas migration in oil-based mud

This section discusses the results obtained from the analysis and interpretation of the DAS, DTS, and DSS data acquired during the tests conducted with oil-based mud. Similar to Test 6 conducted with water, the 10 – 50 Hz frequency range was observed to be the frequency band that best captures the gas signatures and flow dynamics. Hence, this frequency band was selected for visualizing the gas signatures for all the tests conducted with oil-based mud (Figures 15a and 16). The gas migration signatures that were initially buried in the background noise also became more visible in the DSS waterfall plot (Figure 15b) after implementing the signal processing techniques discussed in Chapter 3. Although the top and bottom of the gas are visible on the DAS for test 7 (Figure 15a), the quality of the gas signatures observed on the DSS (Figure 15b) was affected by the loose tube fiber configuration, as previously discussed in the previous chapter. As shown in Figure 16, the implementation of various signal processing techniques greatly improved the visibility of the gas signatures on the DAS data for Tests 1 to 5.

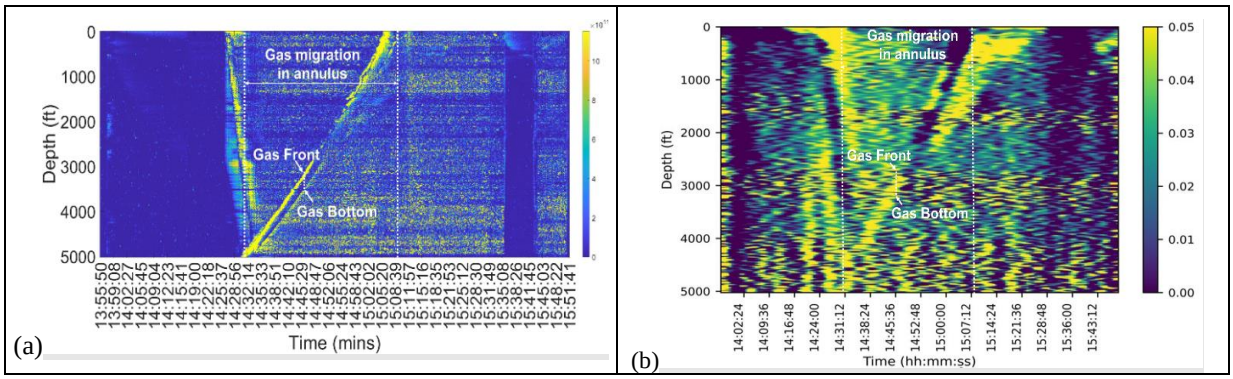

Figure 15. Fiber-optic results for Test 7 (a) DAS FBE [10-50 Hz] (b) Processed DSS (Adeyemi et al. 2023b).

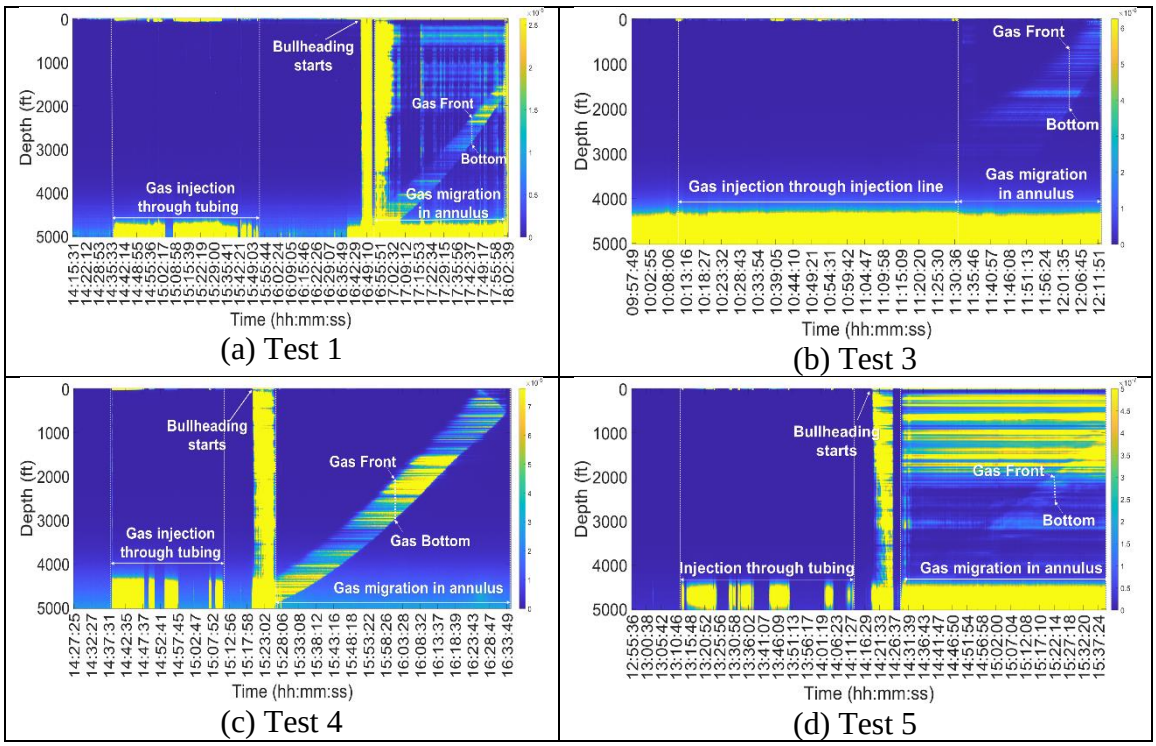

Figure 16. High-frequency DAS FBE waterfall plots corresponding to 10-50 Hz for Tests 1 to 5 (Adeyemi et al. 2023a)

As discussed in Chapter 3, the DAS data was also processed in a low-frequency range (0 – 0.03 Hz) and additional signal processing techniques were also implemented to enhance the visibility of the gas injection signature for Tests 1 to 5. The additional techniques include de-striping, gaussian filtering, and higher-order gradient filtering. The gas injection signature was observed to be more visible on the low-frequency DAS for Tests 1 to 5 (Figures 17a, 17c, 17d), during which injection was done through the tubing. However, the gas injection signature is not

clear for Test 3 (Figure 17b) because the gas injection was done through the half-inch capillary injection line at a very low injection rate (0.25 gpm).

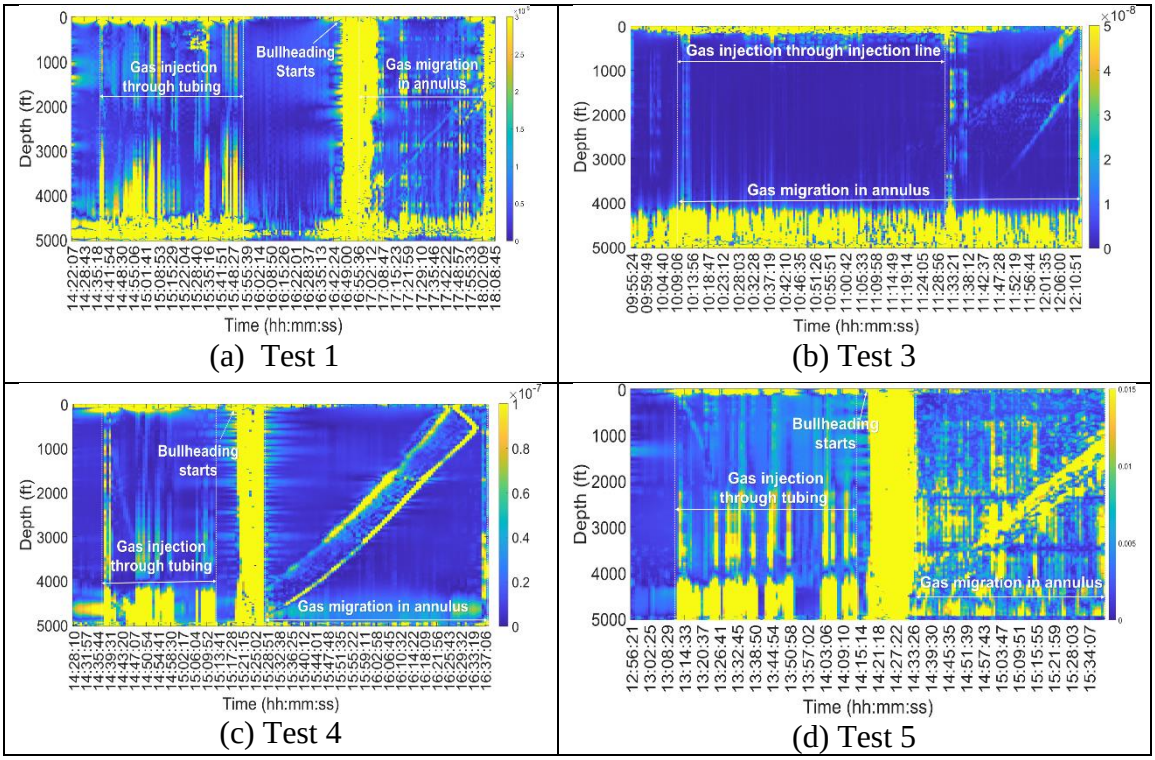

Figure 17. Low-frequency DAS waterfall plots for Tests 1 to 5 (Adeyemi et al. 2023a)

The gas front and bottom velocities (FV and BV) in the oil-based mud were estimated from the F-K signatures at different depths using the processed DAS data. The results of the F-K implementation on the DAS data acquired during the mud tests are shown in Figures 18 to 22. For instances where the F-K signatures were not clear, the FV and BV were estimated manually from the processed DAS data (Figures 15a and 16).

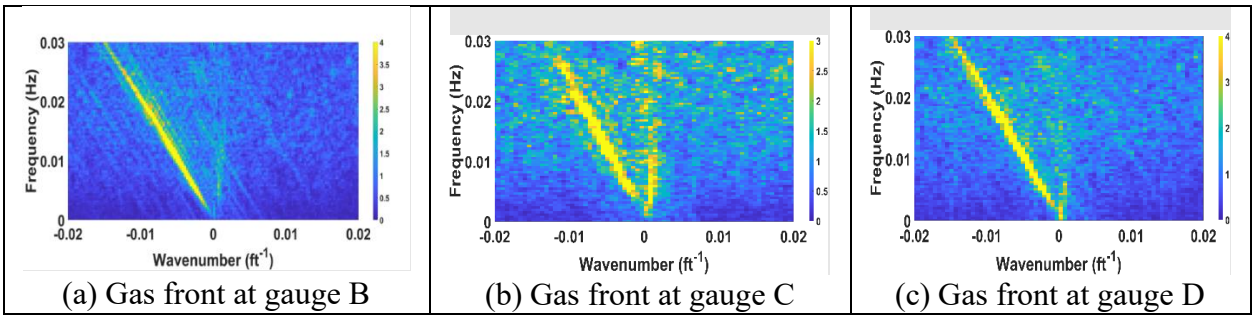

Figure 18. F-K transforms implemented on the DAS data for Test 2 (Adeyemi et al. 2023a).

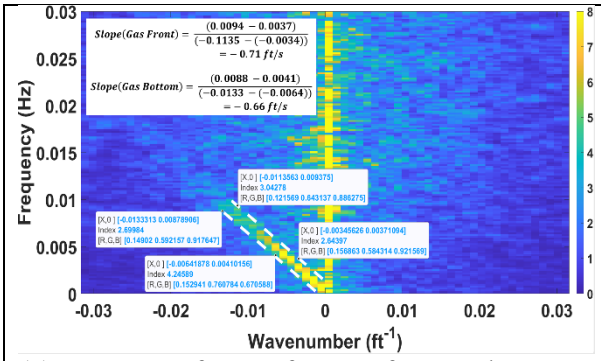

(a) F-K transform of DAS for gas between gauges D-C

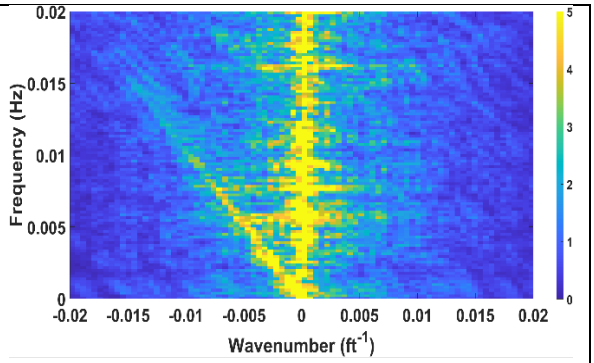

(b) F-K transform of DAS for gas between gauges C-B

Figure 19. F-K transforms implemented on the DAS data and estimated velocities for Test 1 (Adeyemi et al. 2023a).

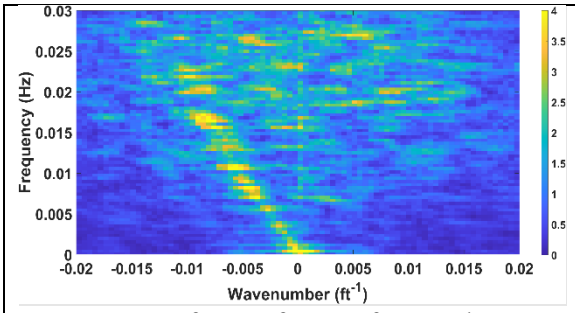

(a) F-K transform of DAS for gas between gauges D-B.

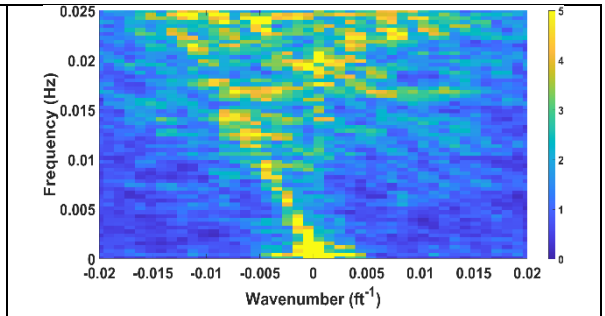

(b)F-K transform of DAS for gas between gauges A- B.

Figure 20. F-K transforms implemented on the DAS data and estimated velocities for Test 3 (Adeyemi et al. 2023a).

The DTS data acquired during Tests 1 to 5 was also processed and analyzed using the approach discussed in Chapter 3. The gas injection and migration signatures are clearly seen from the results obtained (Figures 23a, 23c, 23d). For the same reason as the DAS case, the gas injection signature is not clear for Test 3. The results show that both DAS and DTS can be used to reliably monitor gas behavior and dynamics.

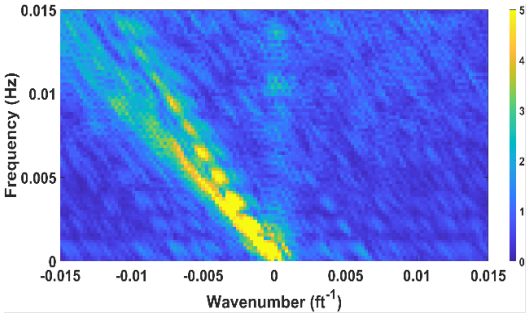

(a) F-K transform of DAS for gas between gauges D-B

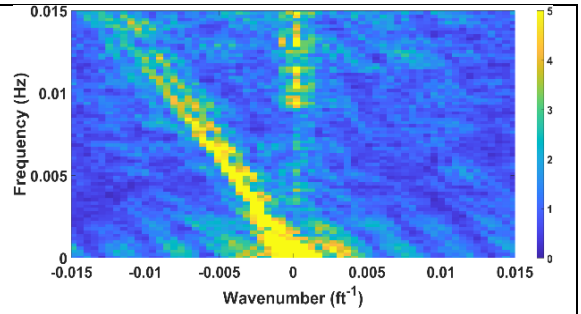

(b)F-K transform of DAS for gas between gauges B-A.

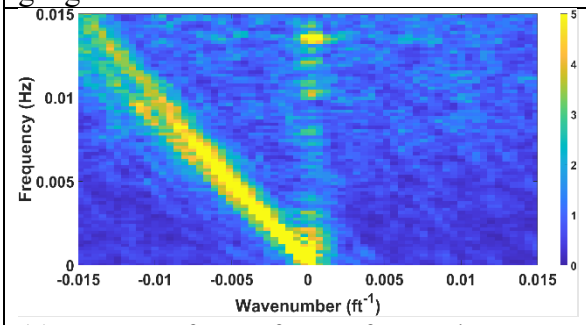

(c) F-K transform of DAS for gas between gauges D-C.

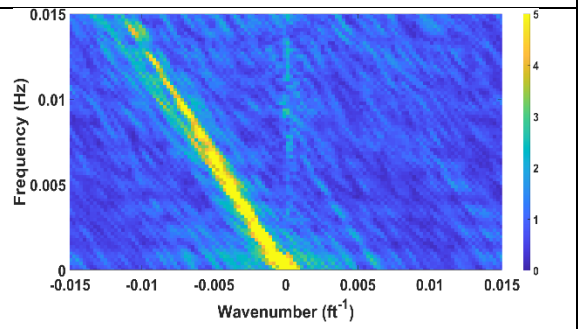

(d) F-K transform of DAS for gas between gauges C-A

Figure 21. F-K transforms implemented on the DAS data and estimated velocities for Test 4 (Adeyemi et al. 2023a).

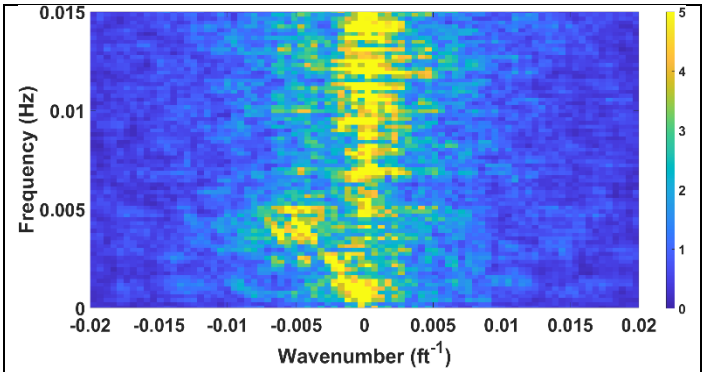

F-K transform of DAS for gas between gauges C-B

Figure 22. F-K transforms implemented on the DAS data and estimated velocities for Test 5 (Adeyemi et al. 2023a).

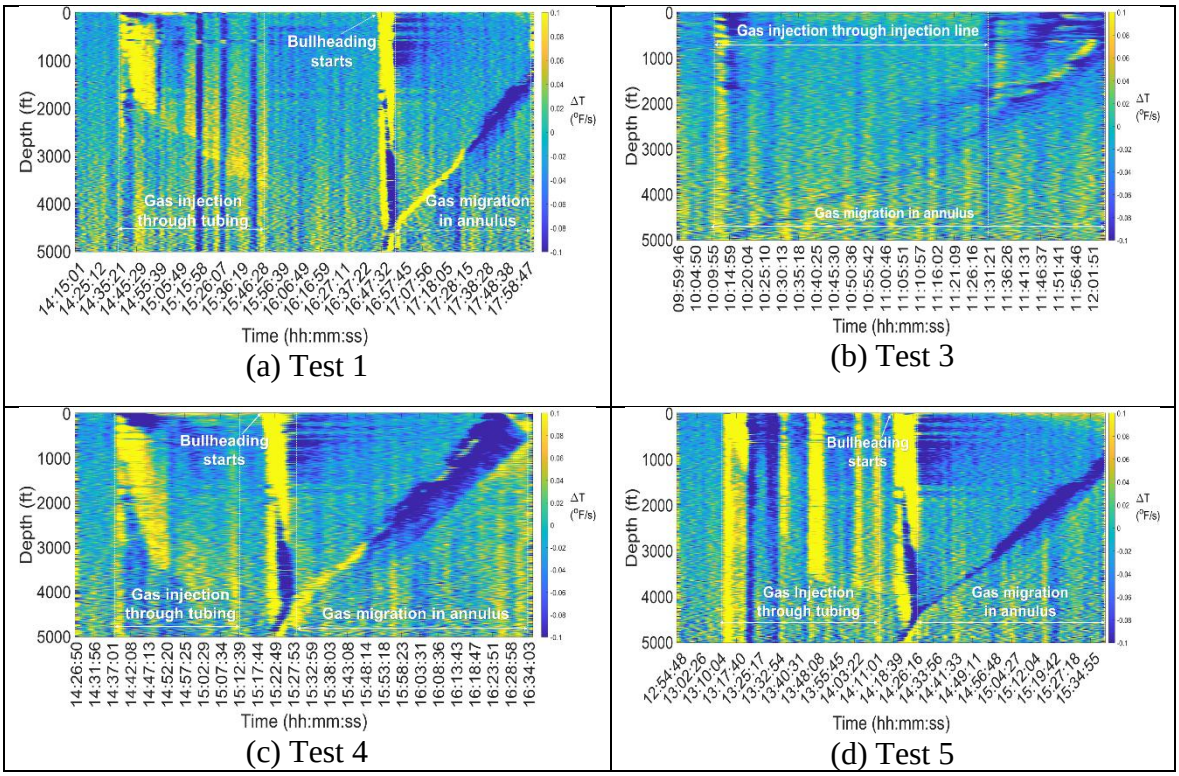

Figure 23. DTS gradient plots for Tests 1 to 5 (Adeyemi et al. 2023a).

To facilitate comparison with the DAS results, the F-K analysis was also implemented on the DTS data for the same time-space window as that of the DAS. The FV and BV were also estimated from the slopes of the F-K signatures obtained from the DTS data. Figures 24 to 27 show the F-K results for the DTS data acquired during Tests 1 to 5. The FV and BV were estimated manually from the DTS waterfall plots (Figure 23) for instances where the F-K signatures were not very clear.

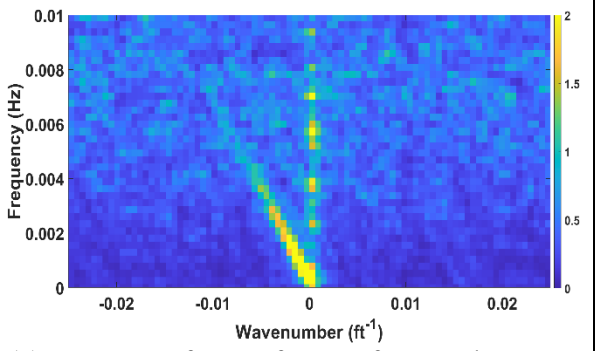

(a) F-K transform of DTS for gas between gauges D-C.

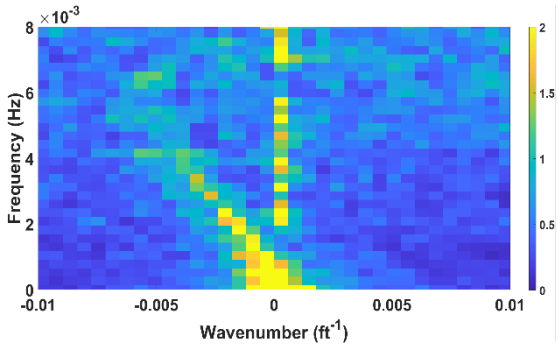

(b) F-K transform of DTS for gas between gauges C-B.

Figure 24. F-K transforms implemented on the DTS data and estimated velocities for Test 1 (Adeyemi et al. 2023a).

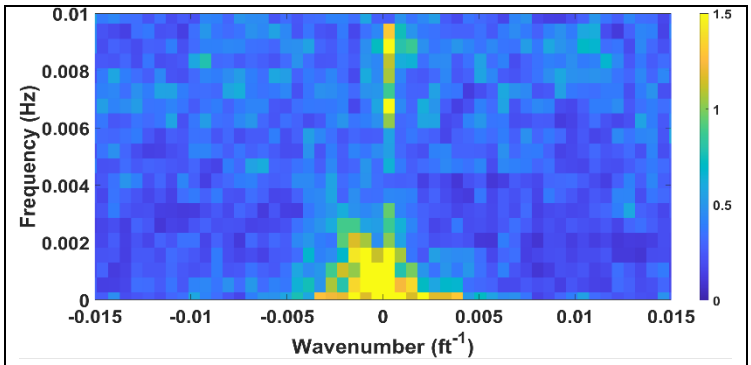

F-K transform of DTS for gas between gauges B-A.

Figure 25. F-K transforms implemented on the DTS data and estimated velocities for Test 3 (Adeyemi et al. 2023a).

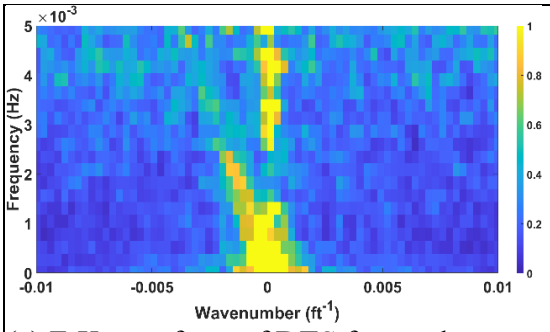

(a) F-K transform of DTS for gas between gauges D-B.

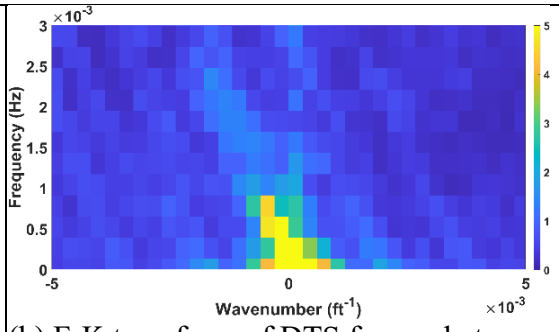

(b) F-K transform of DTS for gas between gauges C-A.

Figure 26. F-K transforms implemented on the DTS data and estimated velocities for Test 4 (Adeyemi et al. 2023a).

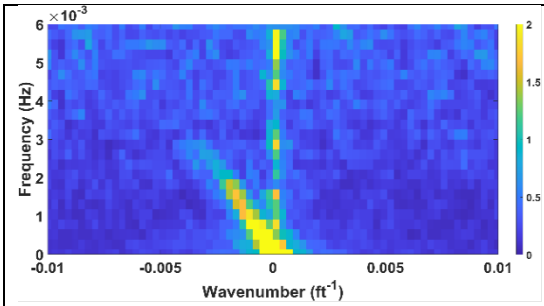

(a) F-K transform of DTS for gas between gauges D-B.

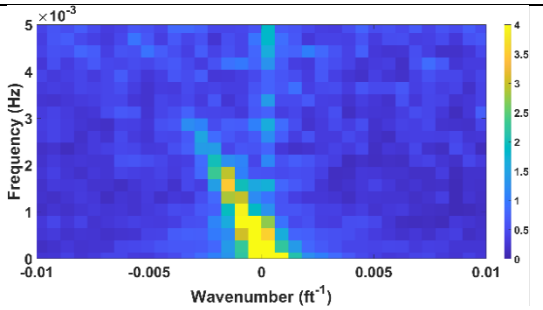

(b) F-K transform of DTS for gas between gauges C-B.

Figure 27. F-K transforms implemented on the DTS data and estimated velocities for Test 5 (Adeyemi et al. 2023a).

The gas rise velocities (FV and BV) and void fractions estimated using DAS and DSS for Test 7 are presented in Table 12. Estimates of the FV and BV were also obtained using downhole gauges (Table 13) and some existing multiphase flow correlations (Table 14). The results presented in Tables 12, 13, and 14 show good agreement between the gas migration velocity estimated independently using DAS and DSS, as well as with downhole gauges and some of the multiphase flow correlations. The results also show that both FV and BV, as well as gas void fraction increase as the gas migrates towards the surface due to a less dominant solubility effect and higher gas expansion effect at lower pressure near the surface. The lengths of the gas-mud region estimated using the fiber-optic data also show a similar trend due to the combined effect of gas solubility and dispersion.

Table 12. DAS and DSS results for Test 7 (Adeyemi et al. 2023b).

Time	**Event**	**DAS**			**DSS**			Gas Void Fraction
		FV (ft/s)	BV (ft/s)	Gas Region Length (ft)	FV (ft/s)	BV (ft/s)	Gas Region Length (ft)	
14:43:50	Gas front at gauge C	1.85	1.80	350	1.81	1.83	344	0.45
14:55:10	Gas front at gauge B	1.94	1.90	449	1.86	1.84	462	0.48
15:04:20	Gas front at gauge A	1.97	1.94	455	1.89	1.86	473	0.50

Table 13. Gauges-based velocities for Test 7 (Adeyemi et al. 2023b).

Gas Location	**Time**	**FV (ft/s)**	**Event**	**Time**	**BV (ft/s)**		**Pressure Drop (psi)**
Gas front at gauge C	14:43:50	1.82	Gas bottom at gauge C	14:46:10	1.75	ΔP_{CB}	53.53
Gas front at gauge B	14:55:10	1.90	Gas bottom at gauge B	14:57:30	1.87	ΔP_{BA}	59.26
Gas front at gauge A	15:04:20	2.05	Gas bottom at gauge A	15:07:05	1.97	ΔP_{DC}	67.17

Table 14. Estimated gas rise velocity for Test 7 using DAS, DSS, and flow correlations (Adeyemi et al. 2023b).

Time	**Event**	**Average Gas Migration Velocity (ft/s)**					
		DAS	DSS	Bubble flow (Griffith 1964)	Bubble flow (Harmathy 1960)	Bubble flow (Zuber and Hench 1962)	Slug flow (Griffith and Wallis 1961)
14:43:50	Gas front at Bank C	1.85	1.80	2.12	1.78	1.58	2.78
14:55:10	Gas front at Bank B	1.94	1.90	2.15	1.79	1.58	2.82
15:04:20	Gas front at Bank A	1.97	1.94	2.17	1.80	1.59	2.86
Mud-Nitrogen Interfacial Tension (σ) = 19.55 dyne/cm, Mud Density (ρ_l) = 8.30 ppg, Annular Geometry Factor (K) = 0.354							

A comparison of the gas FV and BV estimates obtained from the fiber-optic DAS and DTS data (acquired during Tests 1 to 5) with the downhole gauges results is presented in Table 15. It shows the reliability of the fiber-optic sensors for gas dynamics monitoring as the absolute percentage error ranged from 0.79% to 8.53% with a mean error of 3.91%.

Table 15. Comparison of DAS, DTS, and downhole gauges results

Test No.	Velocity Tracked	Gauge Interval	DAS-based Estimates (ft/s)	DTS-based Estimates (ft/s)	Gauges-based Estimates (ft/s)	% Error in DAS-based Estimates	% Error in DTS-based Estimates
1	Gas Front	D-C	0.71	0.66	0.67	7.46 %	1.49 %
		C-B	0.84	0.82	0.87	3.45 %	5.75 %
	Gas Bottom	D-C	0.66	0.61	0.64	1.56 %	4.69 %
		C-B	0.97	0.92	0.94	3.19 %	2.13 %
3	Gas Front	D-B	0.59	0.61	0.64	7.81 %	4.69 %
		B-A	0.88	0.90	0.91	3.30 %	1.09 %
	Gas Bottom	D-B	1.63	1.57	1.52	7.24 %	3.29 %
4	Gas Front	D-B	1.09	1.17	1.11	1.80 %	5.41 %
		B-A	1.27	1.40	1.29	1.55 %	8.53 %
	Gas Bottom	D-C	0.96	0.98	0.95	1.05 %	3.16 %
		C-A	1.28	1.31	1.27	0.79 %	3.15 %
5	Gas Front	D-B	0.84	0.87	0.88	4.55 %	1.14 %
	BV	D-C	0.72	0.63	0.68	5.88 %	7.35 %
		C-B	1.01	1.05	0.99	2.02 %	6.06 %

While both DAS and DTS provided reliable insights into gas behavior and dynamics investigated in this study, I believe it is important to discuss the advantages and limitations of each fiber-optic sensing technique in order to provide some justifications for the deployment of both techniques in this study rather than one of them. DTS has been shown to be more effective for monitoring events that are directly associated with changes in temperature in the wellbore. These include; cooling down during fluid injection, warming back during the shut-in period, and the possibility of a leak along the wellbore, as well as a good indicator of any connection that may exist between the wellbore and a bridge plug (Holley and Kalia 2015; Bhatnagar 2016). DTS also offers some advantages in the area of data handling and processing. For instance, the DTS data acquired in this study was less than 1.0 MB for every 10 seconds of data acquisition. Therefore, the DTS data was easy to handle and process using the available computational systems. Owing

to the type of fiber used (multimode), the DTS was less affected by fiber degradation. Therefore, some events that could not be seen on the DAS due to the fiber degradation effect (for single-mode) are clearly visible on the DTS data. In comparison with the DTS, DAS has been shown to be more sensitive to sudden changes of flow and it is unaffected by the thermal conductivities of the fiber-optic cable and the tubular. DAS has been successfully deployed in some cases where DTS could give wrong information. For instance, DTS could indicate cooling when it is a perforated interval through which there is no fluid influx into the wellbore (Sookprasong et al. 2014; MacPhail et al. 2016). Analysis of the DAS data also provides a more detailed understanding of the dynamic events taking place in the wellbore. Via the implementation of the spectrum and FBE analyses on the DAS data, it is possible to identify the frequency band that captures the individual event and also extract the DAS data that corresponds to the identified frequency band. A major challenge associated with the deployment of DAS is data handling and processing. For instance, the size of DAS data acquired in this study was about 2.0 GB for every 10 seconds. As discussed in Chapter 3, this challenge was overcome via FBE analysis, which serves as an intelligent data compression scheme. In summary, while either DAS or DTS can be deployed to reliably monitor dynamic events in the wellbore, a combination of both techniques is required for a holistic and detailed understanding of the events taking place in the wellbore.

4.2.1. Gas solubility effect

To investigate the effect of gas solubility on gas dynamics in oil-based mud, two additional well-scale experiments were conducted using different gases (nitrogen (Test 8) and helium (Test 9)). As shown in Table 16, the two experiments were conducted at the same injection pressure, bullheading rate, and gas injection volume. The gas injection also took place through the tubing

for both tests. To facilitate direct comparison of results, the same fiber-optic acquisition parameters were also employed for the two tests (Table 4).

Table 16. Well-scale tests matrix for the nitrogen and helium tests.

Wellbore Fluid	Injected Gas	Injection Method	Injection Pressure (psi)	Bullheading Rate (gpm)	Injected Gas Volume (bbl.)
Oil-based mud	Helium	Tubing	2350	250	5.0
Oil-based mud	Nitrogen	Tubing	2350	250	5.0

The DAS data acquired for both tests was processed and analyzed. The FBE analysis discussed in Chapter 3 was implemented on the DAS data for each test. The 0-20 Hz frequency band appears to capture the gas dynamics for both tests. The processed DAS FBE data was then visualized to gain insights into the gas behavior and dynamics during each of the tests. The DAS FBE waterfall plots for the two tests, clearly showing the gas signatures for both tests, are presented in Figure 28. As evident in Figure 28a, the top and bottom are clearly seen up to a depth of about 2120 ft (corresponding to 13:36:46) during the helium test. The lack of visibility of the gas signature beyond that time is due to some technical issues that occurred during the data acquisition, resulting in loss of data. The reverse is the case for the nitrogen test (Figure 28b), where the top and bottom of the gas are only visible up to a depth of 3650 ft (corresponding to 12:38:29). Beyond that time, the gas signatures are observed to have disappeared. The difference in the observations made from the two tests is attributable to the disparity in the degree of solubility of nitrogen and helium in oil-based mud. The nitrogen gas appears to have completely dissolved in the oil-based mud on getting to a depth of 3650 ft and couldn't make it to the surface. However, there is a greater chance that the helium gas will make it to the surface as the gas top and bottom signatures are still clearly

visible at a depth of 2120 ft. The results show that different gases tend to exhibit different degrees of solubility in the oil-based mud.

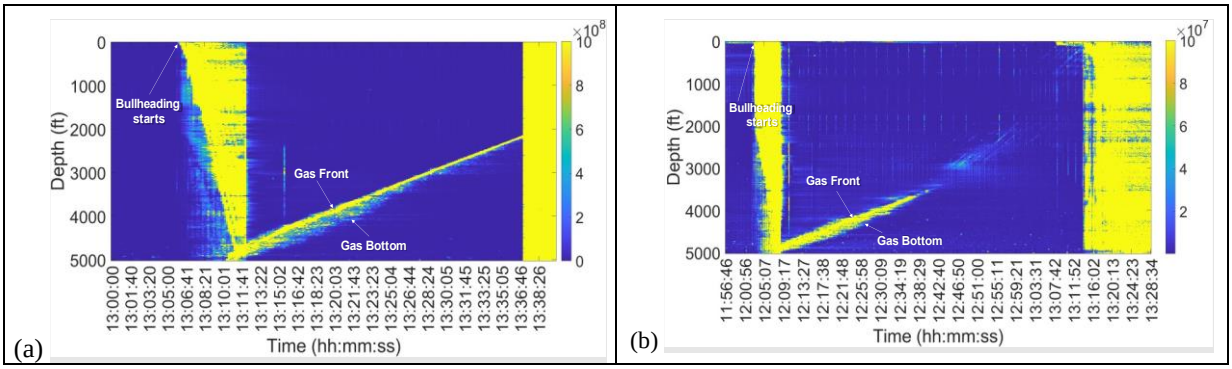

Figure 28. Fiber-optic DAS FBE [0-20 Hz] for (a) Helium and (b) Nitrogen Tests.

4.3. Effects of bottom-hole pressure and gas injection rate on gas dynamics

This section discusses the effects of bottom-hole pressure and gas injection rate on gas dynamics in oil-based mud using the fiber-optic results presented in Table 15. Observation from Table 15 shows that the gas BV between downhole gauges C and D is higher during Test 1 than during Test 4 (conducted at a higher bottomhole pressure). The difference is due to the gas solubility effect in the oil-based mud at different pressures. Gas dissolution in the mud increases with an increase in bottomhole pressure, giving rise to lower gas void fraction and migration velocity. Consequently, a lower gas migration velocity was observed at higher bottomhole pressure. Previous studies have also shown that larger bubbles observable at lower pressures dissolve slower in the mud and tend to migrate at a higher velocity (Ling et al. 2015; Samdani et al. 2023a; He et al. 2022; Dianyuan et al. 2022). The results presented in Table 15 also show that gas migration velocity increases with an increase in injection rate. It is evident from Table 15 that the gas front velocity between gauges D and B during Test 3 is lower than the estimate obtained during Test 4 (conducted at a higher injection rate). This is due to the direct relationship between injection rate and velocity (as described by the continuity equation). A higher gas rise velocity is

therefore expected at a higher gas injection rate. A lower gas injection rate increases the percentage of unsaturated mud available for every barrel of gas injected and this gives rise to faster gas dissolution in the mud. Therefore, the injected gas tends to break into smaller bubbles at a lower injection rate, leading to lower gas migration velocity. This phenomenon was also observed in an experimental investigation conducted by Sun et al. 2019 and it was found to be less pronounced at higher gas injection rates.

4.4. Insights from surface and downhole gauges

4.4.1. Insights from downhole gauges

The results obtained from the use of downhole gauges for real-time tracking of instantaneous gas locations is presented in this section. In Chapter 3, a pressure-drop approach to analyzing downhole gauges for instantaneous gas location determination and gas rise velocity estimation was introduced and schematically illustrated. This approach was employed to analyze the downhole gauges data acquired during Tests 1 to 5. The results of the analysis (showing the instances when the front and bottom of the gas crossed each of the downhole gauges) are presented in Figure 29. The results presented in Figure 29 were combined with the knowledge of the downhole gauges locations to estimate the front and bottom velocities between the downhole gauges during Tests 1 to 5.

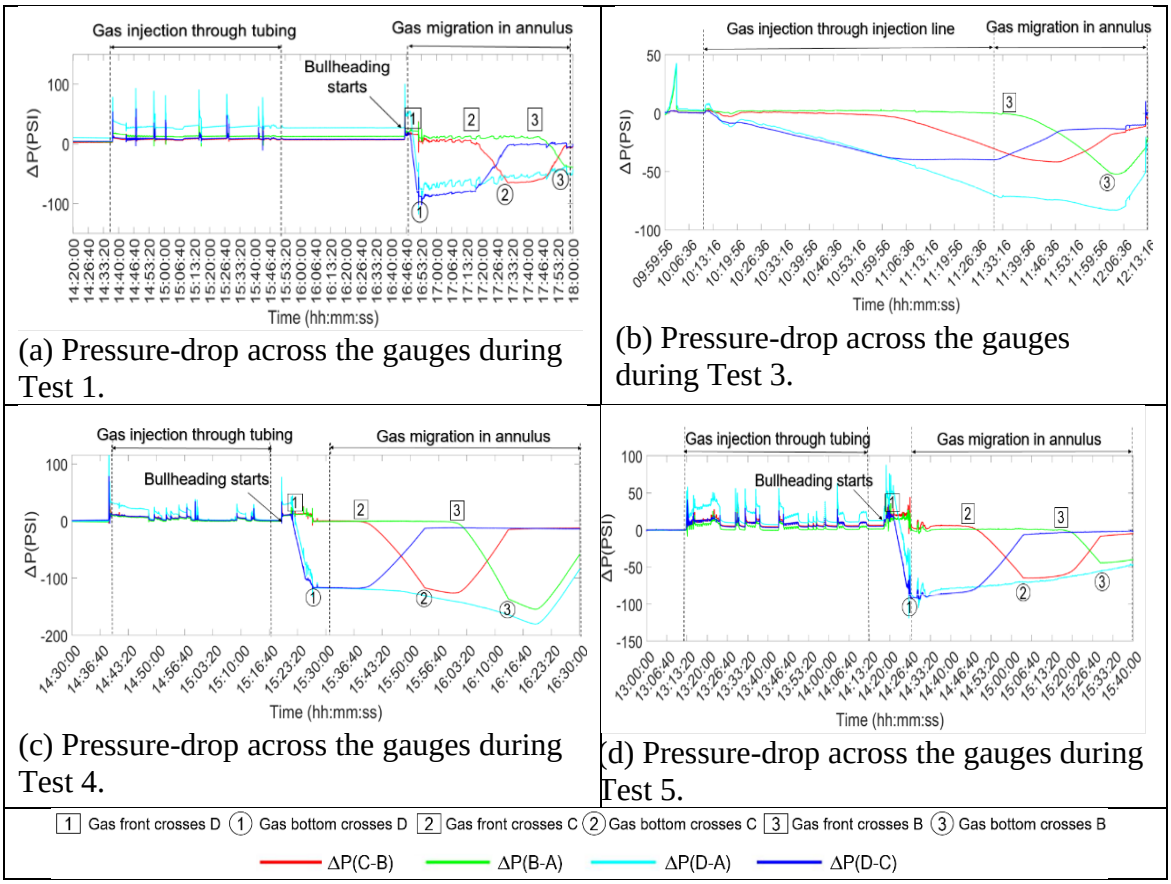

Figure 29. Pressure drop across the downhole gauges for Tests 1 to 5 (Adeyemi et al. 2023a).

4.4.2. Insights from surface gauges

This section describes the usefulness of surface gauges for tracking gas dynamics during injection, bullheading, and migration. The gas injection during Test 1, which took place from 14:36:00 to 15:46:40, is indicated on the surface gauges by a decrease in the pressures of the storage wells 3 and 5 used for the gas injection (Figure 30a). Gas entry into the annulus was also indicated by an increase in the casing pressure. Similar phenomena were also observed from the surface gauge data acquired during Test 4 (Figure 30c). During Test 3, the gas was injected from a gas truck and indicated by an increase in the casing pressure from 10:13:00 to 11:32:50 (Figure 30b). During Test 5 (Figure 30d), the gas was also injected from a truck and confirmed by an increase in the tubing pressure from 13:13:00 to 14:13:00. The surface gauges were also used to estimate the time taken for the injected gas to arrive at the surface. As confirmed by a sudden

increase in the casing pressure, the gas arrived at the surface at 12:06:26 and 16:23:10, during Tests 3 and 4 respectively (Figures 30b and 30c). The insights from the surface gauges were found to be consistent with the observations made from the fiber-optic DAS and DTS (Figures 16 and 23).

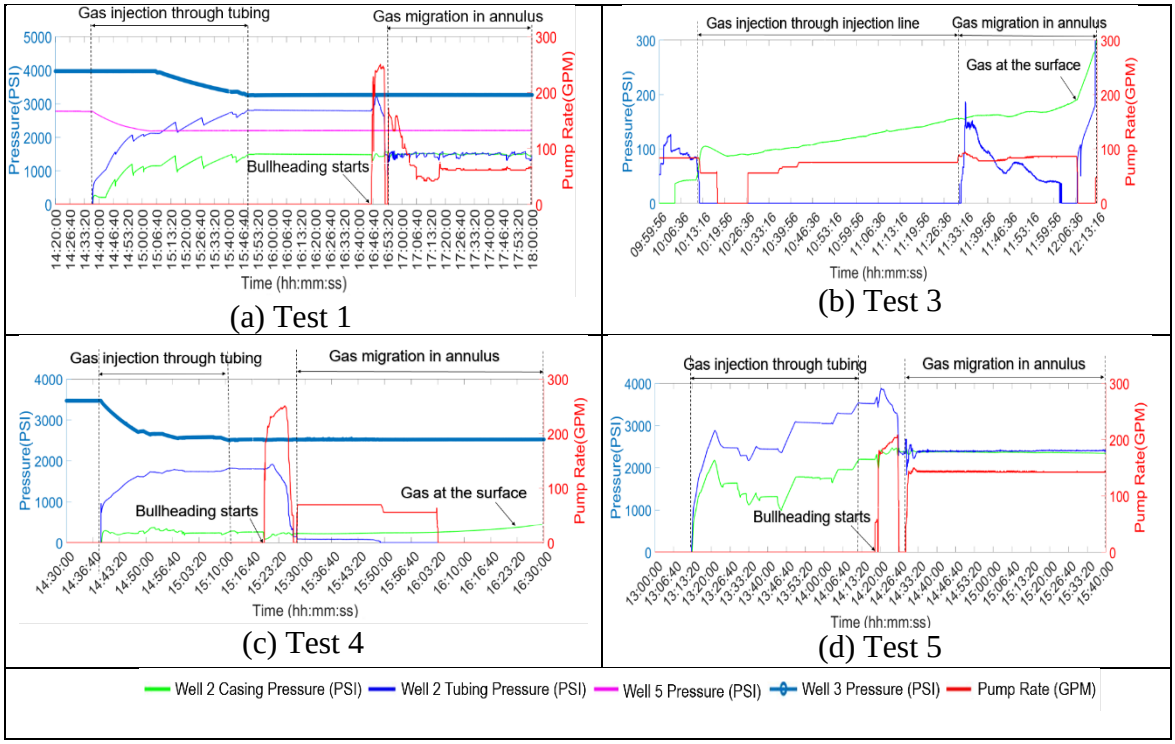

Figure 30. Surface gauge plots for Tests 1 to 5 (Adeyemi et al. 2023a).

Chapter 5. Conclusions and Future Directions

5.1. Conclusions

The main conclusions from this study are summarized below:

- The research demonstrates the successful application of DAS, DTS, and DSS for studying gas behavior and dynamics in oil-based mud at the well-scale .
- The gas front and bottom velocities, void fraction, and length of the gas-affected region that were estimated using each of DAS, DTS, and DSS were observed to show good agreement with the estimates obtained from downhole pressure gauges and some existing multiphase bubble flow correlations.
- The average gas front velocity for nitrogen gas migration in water (Test 6) was found to be slightly higher than that for the oil-based mud conducted at similar gas injection volume, liquid circulation rate, and gas injection method (Test 7). This is due to the gas solubility effect, as more gas tends to dissolve in the oil-based mud, giving rise to a relatively lower migration velocity in the oil-based mud.
- The nitrogen gas dispersion effect is higher in water, accounting for the significantly larger length of the gas-affected region in water than in the oil-based mud.
- At the same injection pressure, bullbeading rate, and injected volume, nitrogen gas tends to exhibit higher solubility in oil-based mud than helium gas.
- A slight disparity exists between the instantaneous gas void fraction estimated in water and oil-based mud. This is due to the initial gas distribution, as well as the effects of phenomena such as gas expansion, dispersion, and solubility.
- The gas migration velocity decreases with an increase in bottomhole pressure due to the effect of gas dissolution in the oil-based mud. Conversely, a direct relationship exists between

injection rate and gas rise velocity as a higher gas injection rate results in a higher gas migration velocity.

5.2. Future Directions

Highlighted below are some other relevant and interesting research areas that could be considered for future studies to extend the results from this research:

- Investigation of the effects of rheological parameters such as plastic viscosity, yield point, apparent viscosity, and gel strength on gas behavior and dynamics in drilling muds.
- Machine-learning-based study of gas behavior in drilling muds for improved well-control operations.
- Understanding of gas dynamics in water and oil-based muds using other gases such as methane.
- Multiphase flow regimes identification and monitoring using distributed fiber-optic sensors.
- Analysis of field results to gain insights into gas behavior and dynamics in an actual field environment.

Appendix. Copyright Information

Please find below the copyright information that permits this author to use some information contained in the papers he had previously published in the Society of Petroleum Engineers (SPE) journals. It is important to note that some information extracted from the previously published journals was significantly modified before they were included in this thesis.

Author-Retained Rights and Terms and Conditions

The term "employers" in the following means the companies*, universities, or an organization for which the authors worked at the time the paper was written.

- Authors/employers retain all intellectual property rights, including any idea, process, procedure, or article of manufacture described in the paper.
- Authors/employers may reproduce and distribute copies of the paper internally to employees of the company* or organization for which the author worked at the time the paper was written without prior SPE approval. Such distribution includes posting of the paper on the employer's intranet accessible only to company employees.
- Authors/employers may reproduce, or authorize reproduction of, and distribute up to 50 paper copies of the paper outside the company or organization for which the author worked at the time the paper was written for personal, business, or educational purposes without prior SPE approval provided that the SPE copyright notice is included. The copies may not be used in any way that implies SPE endorsement of a product or service, and the copies themselves may not be offered for sale.
- Authors/employers may make an oral presentation of the same material without prior SPE approval provided proper acknowledgement of SPE copyright ownership is made.
- Authors/employers may incorporate all or part of the paper in future writings or presentations. If the entire paper or a portion thereof is used in substantially unchanged form, proper acknowledgement of SPE copyright must be made. Authors/employers should locate the paper in OnePetro and follow the "View rights and permissions" link to complete a permissions request.
- Authors/employers may request return of one-time journal publication rights to enable publication of the paper in a non-SPE journal or magazine if the paper is not being considered for publication in an SPE journal. To request permission to publish in a non-SPE periodical, authors should locate the paper in OnePetro and follow the "View rights and permissions" link. Requests for return of one-time journal publication rights will not be granted for papers submitted to SPE for peer review unless the paper is declined for publication or it is at least 6 months after the submission date. If the paper is still in SPE peer review after 6 months and such a request is received, the paper will be withdrawn from SPE peer review.
- In the case of work performed under a U.S. government contract or grant, SPE recognizes that, if the contract/grant so requires, the U.S. government has royalty-free permission to reproduce all or portions of the paper and to authorize others to do so for official U.S. government purposes only.
- For all other uses, authors/employers must request permission from SPE to reproduce or authorize reproduction of the paper. Authors/employers should locate the paper in OnePetro and follow the "View rights and permissions" link to complete a permissions request.
- Although authors are permitted to re-use all or portions of the paper in other works, this does not include granting third-party requests for reprinting, republishing, or other types of re-use. SPE must handle all such third-party requests.

References

Adeyemi, T., Sharma, J., Tabjula, J. 2023. Monitoring and Characterization of Gas Migration in Oil-Based Mud Using Fiber-Optic DAS and DTS. *SPE Journal*, 1-15. https://doi.org/10.2118/217433-PA.

Anfinsin, B. T., Rommetveit, R. 1992. Sensitivity of Early Kick Detection Parameters in Full-Scale Gas Kick Experiments with Oil- and Water-Based Drilling Muds. IADC/SPE 23934 - IADC/SPE Drilling Conference, New Orleans, LA, Feb. 1992.

Aboulrous, A., Alsabagh, A., Abdou, M. 2013. Polymers for circulation loss inhibition of oil well drilling fluids. LAP LAMBERT Academic Publishing.

Baldwin, C. S. 2015. Applications for fiber optic sensing in the upstream oil and gas industry. Proceedings of Fiber Optic Sensors and Applications XII, Maryland, USA, 1–10. 10.1117/12.2176226.

Bhatnagar, A. 2016. Overcoming challenges in fracture stimulation through advanced fracture diagnostics. SPE Asia Pacific Hydraulic Fracturing Conference, Beijing, China, 24-26 August 2016. https://doi.org/10.2118/181802-MS.

Blanc, W., et al. 2022. Distributed fiber optics strain sensors: from long to short distance. *C. R. Géosci.* **354**(S1): 121–143.

Bouali. 2010. A simple and robust destriping algorithm for imaging spectrometers: application to modis data. Presented at the American Society for Photogrammetry and Remote Sensing Conference, San Diego, California, 2010.

Boyd, P.A., Donald, L., Carter, T.S. et al. 1987. Low-viscosity based fluid for low-toxicity oil-mud system. *SPE Drill. Eng*. 2, 218–228.

Casariego, V. and Bourgoyne Jr, A. T. 1988. Generation, migration, and transportation of gas-contaminated regions of drilling fluid. Presented at the SPE Annual Technical Conference and Exhibition, Houston, Texas. October-1988. SPE-18020-MS.

Dewsbury, K., Karamanev, D., Margaritis, A. 1999. Hydrodynamic characteristics of free rise of light solid particles and gas bubbles in non-Newtonian liquids. *Chemical Engineering Science, **54**(21): 4825–4830.* 10.1016/s0009-2509(99)00200-6.

Ekechukwu, G. K. and Sharma, J. 2021. Well-Scale Demonstration of Distributed Pressure Sensing Using Fiber-Optic DAS and DTS. *Sci Rep* **11** (1): 12505. https://doi.org/10.1038/s41598-021-91916-7.

Ekechukwu, G. and Sharma, J. 2023. Degradation Analysis of Single-Mode and Multimode Fibers in a Full-Scale Wellbore and Its Impact on DAS and DTS Measurements. *IEEE Sensors Journal*, **23**(9): 9287-9300. 10.1109/JSEN.2023.3257264.

Feo, G., Sharma, J., Kortukov, D. et al. 2020. Distributed Fiber Optic Sensing for Real-Time Monitoring of Gas in Riser during Offshore Drilling. *Sensors (Basel)* **20** (1). https://doi.org/10.3390/s20010267

Griffith, P. 1964. The prediction of low-quality boiling void. *J. Heat Tran*. 86, 327–33. https://doi.org/10.1115/1.3688684.

Griffith, P., Wallis, G.B. 1961. Two-phase slug flow. *J. Heat Tran*. 83, 307–320. https:// doi.org/10.1115/1.3682268.

Haddad, R. A. and Akansu, A. N. 1991. A Class of Fast Gaussian Binomial Filters for Speech and Image Processing. *IEEE Trans Signal Process* **39** (3): 723–727. https://doi.org/10.1109/78.80892.

Harmathy, T. Z. 1960. Velocity of Large Drops and Bubbles in Media of Infinite or Restricted Extent. *AIChE J* **6** (2): 281–288. https://doi.org/10.1002/ aic.690060222.

Holley, E. H., Kalia, N. 2015. Fiber-optic monitoring: Stimulation results from unconventional reservoirs. Unconventional Resources Technology Conference, San Antonio, Texas, 20-22 July 2015. SPE-196074- MS

Jayah, M. N., Aziz, I. A., Drus, Z. et al. 2013. Integrated Technology Approach to Explore Carbonate Reservoirs in Malaysia Enhances PMCD Potentials and Enables Successful Prospect Evaluations. Paper presented at the IADC/SPE Managed Pressure Drilling and Underbalanced Operations Conference and Exhibition, San Antonio, Texas, USA, 17–18 April. SPE-164576-MS. https://doi.org/10.2118/164576-MS

Johnson, A., Rezmer-Cooper, I., Bailey, T. et al. 1995. Gas Migration: Fast, Slow or Stopped. Paper presented at the SPE/IADC Drilling Conference, Amsterdam, Netherlands, 28 February –2 March. SPE-29342-MS. https://doi.org/10.2118/29342-MS.

Kunju, M. and Mauricio, A. 2023a. Comparison of Riser Gas Unloading in Water and SBM: Full-Scale Experiments. Paper presented at the SPE Latin American and Caribbean Petroleum Engineering Conference, Port of Spain, Trinidad and Tobago, June 14 – 15. https://doi.org/10.2118/213195-MS

Kunju, M. and Mauricio, A. 2023b. Analysis of Riser Gas Pressure from Full-Scale Gas-in-Riser Experiments with Instrumentation. *SPE Drill & Compl* **38:** 170–186. https://doi.org/10.2118/206389-PA.

Khshi-Tafti, E., Kumar, R., Cho, H. 2011. Measurement of surface interfacial tension as a function of temperature using pendant drop images. *Int J Optomechatronics* **5**(4):393 - 403.

Kogure, T., Okuda, Y. 2018. Monitoring the vertical distribution of rainfall-induced strain changes in a landslide measured by distributed fiber optic sensing with Rayleigh backscattering. *Geophys. Res. Lett*. 45, 4033-4040.

Kunju, M., Adeyemi, T., Sharma, J. et al. 2023. Fixed Choke Constant Outflow Circulation Method for Riser Gas Handling : Full-Scale Tests in Water- and Synthetic-Based Mud with Gauges and Distributed Fiber-Optic Sensors. *SPE Journal, 1-19.* https://doi.org/10.2118/217444-PA.

Leandro, V., Roni, A., André, L. 2014. Impact of Gas Solubility on Kick Detection in N-Paraffin Based Drilling Fluids. 2014 AADE Fluids Technical Conference and Exhibition held at the Hilton Houston North Hotel, Houston, Texas, April 15-16.

Li, B., Luo, L., Yu, Y. et al. 2017. Dynamic Strain Measurement Using Small Gain Stimulated Brillouin Scattering in STFT-BOTDR. *IEEE Sensors* **17** (9) : 2718-2724. 10.1109/JSEN.2017.2657119.

Li, H., Ji, H., Huang, Z. et al. 2016. A New Void Fraction Measurement Method for Gas-Liquid Two-Phase Flow in Small Channels. *Sensors* **16**(2): 159. https://doi.org/10.3390/s16020159.

Liu, Y., Ozbayoglu, E. M., Upchurch, E. R. et al. 2023a. Computational Fluid Dynamics Simulations of Taylor Bubbles Rising in Vertical and Inclined Concentric Annuli. *Int J Multiph Flow* 159: 104–333. https://doi.org/10.1016/j.ijmultiphaseflow.2022.104333.

Liu, Y., Upchurch, E. R., and Ozbayoglu, E. M. 2021. Experimental Study of Single Taylor Bubble Rising in Stagnant and Downward Flowing Non-Newtonian Fluids in Inclined Pipes. *Energies* 14 (3): 578. https://doi.org/10.3390/en14030578.

Li, H., Mouline, Y., Midoux, N. 2002. Modelling the bubble formation dynamics in non-Newtonian fluids. *Chemical Engineering Science, **57(**3), 339–346.* doi:10.1016/s0009-2509(01)00394-3.

Lou, W., Wang, Z., Guo, B. et al. 2021. Numerical Analysis of Velocity Field and Energy Transformation, and Prediction Model for Taylor Bubbles in Annular Slug Flow of Static Power Law Fluid. *Chem Eng Sci* 250. https://doi.org/10.1016/j.ces.2021.117396.

Liu, Y., Upchurch, E. R., Ozbayoglu, E. M. et al. 2023b. Gas Migration Model for Non-Newtonian Fluids Under Shut-In Well Conditions. Paper presented at the SPE/IADC International Drilling Conference and Exhibition, Stavanger, Norway, 7–9 March. SPE-212466-MS. https://doi.org/10.2118/212466- MS.

Liu, Y., Upchurch, E. R., Ozbayoglu, E. M. et al. 2023c. Design and Calculation of Process Parameters in Bullheading and Pressurized Mud Cap Drilling. Paper presented at the SPE/IADC International Drilling Conference and Exhibition, Stavanger, Norway, 7–9 March. SPE-212455-MS. https://doi.org/ 10.2118/212455-MS

MacPhail, W., Kirkpatrick, J., Banack, B. et al. 2016. SAGD Production Observations Using Fiber Optic Distributed Acoustic and Temperature Sensing: SAGD DAS-Listening To Wells.

Manikonda, K., Hasan, A. R., Kaldirim, O. et al. 2019. Understanding Gas Kick Behavior in Water and Oil-Based Drilling Fluids. Paper presented at the SPE Kuwait Oil & Gas Show and Conference, Mishref, Kuwait, 13–16 October. SPE-198069-MS. https://doi.org/10.2118/198069-MS.

Miyabayashi, K., et al. 2022. Slug Length Estimation for Gas-liquid Slug Flow in T-shaped Microdevices with Liquid Film. *IFAC-PapersOnLine* **55** (7): 210-215. https://doi.org/10.1016/j.ifacol.2022.07.446.

Nwaka, N., Wei, C., Chen, Y. 2020a. A Simplified Two-Phase Flow Model for Riser Gas Management with Non-Aqueous Drilling Fluids. *Journal of Energy Resources Technology* **142**(10): 1-27.

Nwaka, N., Wei, C., Ambrose, A. et al. 2020b. Gas in riser: On modeling gas influxes in non-aqueous drilling fluids with time-dependent desorption considerations. *Journal of Petroleum Science and Engineering* **195**: 107785.

O'Brien, T. B. 1981. Handling Gas in an Oil Mud Takes Special Precautions. *World Oil*, 22-29.

Perry, S., Wei, C., Chen, Y. 2020. Absorption Kinetics of Gas Influxes into Nonaqueous Fluids During Riser Gas Handling Events. AADE 2020 Fluids Technical Conference, Marriott Marquis, Houston, Texas, April 14-15, 2020.

Pietrzak, M., Płaczek, M. Void fraction predictive methods in two-phase flow across a small diameter channel. *Int. J. Multiph. Flow* 121, 103-115. 10.1016/j.ijmultiphaseflow.2019.103115.

Poettman, H., and Paul, G. 1952. The multiphase flow of gas, oil, and water through vertical flow strings with application to the design of gas-lift installations. Drilling and production practice. American Petroleum Institute, 1952.

Rader, D. W., Bourgoyne, A. T., and Ward, R. H. 1975. Factors Affecting Bubble-Rise Velocity of Gas Kicks. *J Pet Technol* 27 (5): 571–584. SPE-4647- PA. https://doi.org/10.2118/4647-PA.

Rao, S. S., Samdani, G. A., Penny, G. et al. 2022. Pilot-Scale Experimental Study of Gas Migration in Wellbores. Paper presented at the SPE Annual Technical Conference and Exhibition, Houston, Texas, USA, 3–5 October. SPE-210137-MS. https://doi.org/10.2118/210137-MS.

Samdani, G. A., Rao, S. S., Moganaradjou, Y. et al. 2023a. Gas Migration in PMCD Operations: Instrumented Well Study Provides Fundamental Insights. Paper presented at the SPE/IADC International Drilling Conference and Exhibition, Stavanger, Norway, 7–9 March. SPE-212546-MS. https://doi.org/ 10.2118/212546-MS.

Samdani, G. A., Rao, S. S., Moganaradjou, Y. et al. 2023b. Gas Bullheading Study in an Instrumented Well. Paper presented at the SPE/IADC International Drilling Conference and Exhibition, Stavanger, Norway, 7–9 March. SPE-212477-MS. https://doi.org/10.2118/212477-MS.

Sang, H.W., Zhang, D., Gao, Y.L., et al., 2019. Strain distribution based geometric models for characterizing the deformation of a sliding zone. *Eng. Geol.* **263**: 105300. https://doi.org/10.1016/j.enggeo.2019.105300.

Santos, O. L., Williams, W. C., Sharma, J. et al. 2021. Use of Fiber Optic Information to Detect and Investigate the Gas-in-Riser Phenomenon. Paper presented at the SPE/IADC International Drilling Conference and Exhibition, Virtual, 8–12 March. SPE-204115-MS. https://doi.org/10.2118/204115- MS.

Santos, O.L., Almeida, M., Sharma, J. et al. 2023. New Experimental Results Show the Application of Fiber Optic to Detect and to Track Gas Position in Marine Risers and Shed Light on the Gas Migration Phenomenon Inside a Closed Well. *SPE Drill & Compl* **38**: 34–51. https://doi.org/10.2118/208682-PA.

Santos, O. L., Almeida, M., Sharma, J. et al. 2022. New Experimental Results Show the Application of Fiber Optic to Detect and to Track Gas Position in Marine Risers and Shed Lights on the Gas Migration Phenomenon Inside a Closed Well. Paper presented at the IADC/SPE International Drilling Conference and Exhibition, Galveston, Texas, USA, March 2022. https://doi.org/10.2118/208682-MS.

Sasaki, T., Park, J., Soga, K. et al. 2019. Distributed Fiber Optic Strain Sensing of an Axially Deformed Well Model in the Laboratory. *J. Nat. Gas Sci. Eng*. **72** : 103028. https://doi.org/10.1016/j.jngse.2019.103028.

Sharma, J., Cuny, T., Ogunsanwo, O. et al. 2021. Low-Frequency Distributed Acoustic Sensing for Early Gas Detection in a Wellbore. *IEEE Sensors* J **21** (5): 6158–6169. https://doi.org/10.1109/JSEN.2020.3038738.

Sharma, J., Santos, O. L. A., Feo, G. et al. 2020. Well-Scale Multiphase Flow Characterization and Validation Using Distributed Fiber-Optic Sensors for Gas Kick Monitoring. *Opt Express* **28** (26): 38773–38787.

Sookprasong, P. A., Gill, C. C., Hurt, R. S. 2014. Lessons learned from das and dts in multicluster, multistage horizontal well fracturing: interpretation of hydraulic fracture initiation and propagation through diagnostics. IADC/SPE Asia Pacific Drilling Technology Conference, Bangkok, Thailand, 25-27 August 2014. https://doi.org/10.2118/170512-MS.

Tabjula, J. L., Wei, C., Sharma, J. et al. 2023. Well-Scale Experimental and Numerical Modeling Studies of Gas Bullheading Using Fiber-Optic DAS and DTS. *Geoenergy Science and Engineering* **225**: 211662. https://doi.org/10.1016/j.geoen.2023.211662.

Thomas, D. C., Lea., J. F., Turek, E. A. 1982. Gas Solubility in Oil-Based Drilling Fluids: Effects on Kick Detection. SPE 57th Annual Fall Technical Conference and Exhibition, New Orleans, LA, Sep. 1982.

Ugueto, G., Wojtaszek, M., Mondal, S. et al. 2021. New Fracture Diagnostic Tool for Unconventionals: High-Resolution Distributed Strain Sensing via Rayleigh Frequency Shift during Production in Hydraulic Fracture Test 2. Proceedings of the 9th Unconventional Resources Technology Conference, Houston, TX (United States), 26-28 July 2021.

Wang, Q., Xiaodong J., Mi W. et al. 2019. Bubble mapping: three-dimensional visualization of gas–liquid flow regimes using electrical tomography. *Measurement Science and Technology* **30**(4): 045303.

Wei, C. and Chen, Y. 2022b. Improved Understanding of Gas Influx Behaviors During Riser Gas Events: A Data Assimilation Approach. AADE 2022 Fluids Technical Conference, Houston, Texas, April 19-20, 2022.

Wei, C., Tabjula, J. L., Sharma, J. et al. 2023a. A Novel Data Assimilation-Based Real-Time State Estimation Method for Gas Influx Profiling During Riser Gas Events. *ASME. J. Energy Resour. Technol*. **145**(9): 092901.

Wei, C. and Chen, Y. 2023. A study of the fixed choke and constant outflow method for riser gas handling. *Process Safety and Environmental Protection* **174**: 756-769.

Wei, C., Tabjula, J., Sharma, J., Chen, Y. 2023b. The Modeling of Two-way Coupled Transient Multiphase Flow and Heat Transfer during Gas Influx Management using Fiber Optic Distributed Temperature Sensing Measurements. *International Journal of Heat and Mass Transfer*, **214**(124447):47. 10.1016/j.ijheatmasstransfer.2023.124.

Williams, W. C., Taylor, C. E., Almeida, M. A. et al. 2020. Distributed Sensing and Real Time Visualization of Gas Kick Dynamics in a Full-Scale Wellbore. Paper presented at the SPE Annual Technical Conference and Exhibition, Virtual, October 26 - 29. https://doi.org/10.2118/201539-MS

Xu, Z., Song, X., Li, G. et al. 2019. Gas kick simulation in oil-based drilling fluids with the gas solubility effect during high-temperature and high-pressure well drilling. *Applied Thermal Engineering* 149, 1080 -1097.

Yoshida, N., Satoshi, K., Iwao, S. et al. 2002. Equivalent linear method considering frequency dependent characteristics of stiffness and damping. *Soil Dynamics and Earthquake Engineering* **22**: 205 – 222.

Zhang, Q. M., Zhu, P. Y., Wang, S. L. et al. 2010. Research of BOTDR on Dike Strain Monitoring. *Applied Mechanics and Materials.* **36:** 187–191.

Zhang, Y., Lei, X., Hashimoto, T. et al. 2021. Toward retrieving distributed aquifer hydraulic parameters from distributed strain sensing. *Journal of Geophysical Research: Solid Earth*. **126**(1): e2020JB020056. https://doi. Org/10.1029/2020JB02005.

Zhang, Y., Xue, Z. 2019. Deformation-Based monitoring of water migration in rocks using distributed fiber optic strain sensing: a laboratory study. *Water Resources Research,* 55, 8368–8383. https://doi. org/10.1029/2019WR024795

Zuber, N. and Findlay, J.A. 1965. Average Volumetric Concentration in Two-Phase Flow Systems. *Journal of Heat Transfer* **87**(4): 453-468.

Zuber, N, Hench, J. 1962. Steady State and Transient Void Fraction of Bubbling Systems and Their Operating Limit. Part 1: Steady State Operation. *General Electric Report*. No. 62GLl00, July 1962.

Vita

Temitayo Sheriff Adeyemi, born in Ogun state, Nigeria, completed a bachelor's degree in Petroleum Engineering (with First Class Honors) from the University of Ibadan, Nigeria. After his undergraduate study, he worked as a Graduate Teaching Assistant at Ekiti State University (EKSU) in Nigeria before traveling to the United States for his master's degree in Petroleum Engineering at the Craft and Hawkins Department of Petroleum Engineering, Louisiana State University, Baton Rouge. Upon completion of his master's degree, he will begin work on his doctorate.